Chapter 3
Combining Scanning Probe Microscopy and Transmission Electron Microscopy

Alexandra Nafari, Johan Angenete, Krister Svensson, Anke Sanz-Velasco, and Håkan Olin

Abstract This chapter is a review of an in situ method where a scanning probe microscope (SPM) has been combined with a transmission electron microscope (TEM). By inserting a miniaturized SPM inside a TEM, a large set of open problems can be addressed and, perhaps more importantly, one may start to think about experiments in a new kind of laboratory, an in situ TEM probing laboratory, where the TEM is transformed from a microscope for still images to a real-time local probing tool. In this method, called TEMSPM, the TEM is used for imaging and analysis of a sample and SPM tip, while the SPM is used for probing of electrical and mechanical properties or for local manipulation of the sample. This chapter covers both instrumental and applicational aspects of TEMSPM.

Abbreviations

a-C	Amorphous carbon
AFM	Atomic force microscopy/microscope
CBED	Convergent beam electron diffraction
EBID	Electron beam induced deposition
ED	Electron diffraction
EDS	Energy dispersive X-ray spectroscopy
EELS	Electron energy loss spectroscopy
EFTEM	Energy filtered transmission electron microscopy/microscope
FIB	Focused ion beam
HREM	High resolution electron microscopy
HRTEM	High resolution transmission electron microscope
MEMS	Micro-electro-mechanical systems
NEMS	Nano-electro-mechanical systems
REM	Reflection electron microscopy
SAED	Selected area electron diffraction
SEM	Scanning electron microscopy/microscope

Published in SCANNING PROBE MICROSCOPY IN NANOSCIENCE AND NANOTECHNOLOGY 2
NanoScience and Technology, 2011, Part 1, 59-99,
DOI: 10.1007/978-3-642-10497-8_3

SPM	Scanning probe microscopy/microscope
STEM	Scanning transmission electron microscopy/microscope
STM	Scanning tunneling microscopy/microscope
SWNT	Single-wall nanotube
TEM	Transmission electron microscopy/microscope
TEMAFM	Combined TEM and AFM
TEMSPM	Combined TEM and SPM
TEMSTM	Combined TEM and STM

3.1 Introduction

3.1.1 Why Combine SPM and TEM?

The transmission electron microscope (TEM) is the only currently available method that offers sub-nanometer resolution imaging at high frame rates: TV rate or faster. As such, it offers unique possibilities for detailed and real-time observation of the probe–sample interaction in scanning probe microscopy (SPM).

Firstly, in standard SPM, the tip shape and tip–sample distance is usually unknown. By combining SPM with TEM, the imaging capability of the TEM can be used to monitor the positioning of the SPM probe relative to the sample. In this way, the approach can be controlled to avoid unintentional contact between probe and sample. The TEM monitoring is a powerful tool especially in cases when a particular feature of the sample needs to be found or a specific location of the sample should be investigated. In cases where the probe may have an irregular shape (which is the case with many STM tips), it may be of importance to control which part of the tip approaches the sample first. Moreover, because electrostatic and chemical forces between the tip and sample are highly dependent on the radius of the tip and the tip–sample distance, and, as we will see later, using TEM to image the tip and sample during an experiment yields surprising findings. The TEM imaging can also be used to extract the contact area between the tip and sample, which is of importance when studying the fundamentals of friction or the electrical conductance of point contacts.

Besides using the TEM as a monitoring tool for positioning and approach, it can also be used to extract complementary information, not accessible by SPM alone. The TEM can be used to follow changes in the physical properties of the sample and probe as functions of experimental parameters, such as field and current in the STM case, or force in the AFM case. Furthermore, with the imaging capabilities of TEM, morphological or structural information of the sample and/or the probe can be collected, for example, to detect the existence of an oxide layer on the probe or sample, or to observe whether the shape of the tip remains unchanged during an experiment. On a more detailed level, by using electron diffraction (ED) methods or high resolution TEM (HRTEM), it is also possible to investigate the crystallographic

properties of the probe and the sample, such as phase changes due to resistive heating or mechanical deformation. The TEM also offers a variety of spectroscopic analysis techniques, of which energy dispersive X-ray spectroscopy (EDS), electron energy loss spectroscopy (EELS), and energy filtered TEM (EFTEM) are the most predominant methods. With these, information about the chemical composition and electronic structure can be extracted. Such chemical information is hard to obtain by SPM methods alone. This additional information is very useful during an SPM experiment for confirmation of the sample phase or to follow phase changes or diffusion and electromigration processes, to give a few examples. A third way to utilize the combination of SPM and TEM is to use the SPM to manipulate a sample inside the TEM. Such manipulation could include resistive heating to clean away an oxide layer, picking up and move nanoobjects with the probe or using the probe to mechanically deform the sample in a controlled way, and analyze the mechanical response.

The TEMSPM has been used for almost two decades, however, there is still no generally accepted nomenclature for this method. There are many in situ TEM techniques such as chemical reactions, heating, cooling, or optical detection that are not combined with scanning probe instruments. Takayanagi and co-workers coined the term TEM–STM [1, 2] for their early in situ experiments and this was used by several groups and later a related technique was called TEM–AFM [3]. But there are also variants such as STM–TEM [4, 5], in situ TEM probing, or TEM–SPM. Therefore, to differentiate truly combined SPM and TEM technology from other in situ TEM techniques and to facilitate literature studies in the field, we propose that the term "TEMSPM" is used when referring to the use of SPM methods combined with TEM, regardless of whether or not the SPM instrument is used in scanning or point probing mode. In more specific cases, the terms "TEMSTM and TEMAFM" can be used, and "TEMSPM" should be viewed as the general family of the techniques. Note that the acronyms now are without hyphen. This is in analogy with naming conventions that give names like HRTEM (High-Resolution TEM) but also, and this is of some importance, it will facilitate literature search. When a hyphen is used, most search machines will return results not only with, for example TEM–STM, but also studies where the two methods are used separately.

In this chapter, work done in the field of combining SPM methods with TEM will be reviewed. There are no other reviews covering the full spectrum of the TEM-SPM method, however, Wang et al. have made several reviews on their extensive early TEMSPM work [6–9]. Furthermore, Golberg et al. have published a review on their recent work on characterizing various nanotube materials using the TEMSPM technique [10] and Nelson et al. have reviewed the nanorobotic aspects of carbon nanotubes [11–13]. A special issue of the MRS bulletin reviewed general in situ TEM techniques [14], including a section on TEMSPM. In a review published by Kociak et al. [15], the possibilities of a TEM nanolaboratory were elaborated on and a book on general in situ TEM techniques edited by Banhart can be found in [16]. Although this chapter aims to provide a comprehensive report of methods related to the TEMSPM technique, two related in situ electron microscopy probing methods are not covered: in situ TEM nanoindentation and probing in scanning electron

microscopes (SEM). Further information about the in situ TEM nanoindentation is available in reviews by Stach et al. [17–19], and probing experiments inside SEM are, among others, reviewed in [20].

3.2 Some Aspects of TEM Instrumentation

The imaging principle in TEM is based on the transmission of an electron beam through a thin sample. As the electrons interact with the sample during their passage through it, the transmitted beam carries information from the sample. This information can be extracted as images, diffractograms, or spectra and, often after some interpretation, be used for analysis of the sample structure and composition. The electron beam is generated by an electron gun, and the beam is formed by a series of apertures and magnetic lenses before and after the passage through the sample. The TEM sample thickness must be kept small in order to allow electron transmission through it. The optimum sample thickness depends on several factors such as sample composition, mode of analysis, and acceleration voltage of the TEM, and typically, the thickness is in the range of 20–300 nm.

In most TEM instrument designs, the sample is mounted into a specimen holder, which basically consists of a 20–40 cm long rod, as shown in Fig. 3.1. The sample is supported by a device at the end of the rod, and the rod itself is entered through a vacuum port on the side of the TEM instrument so that the sample is oriented perpendicular to the electron beam. Inside standard TEM instruments, space is limited and the most limiting factor for an in situ TEM instrument is the space available between the two pole pieces of the objective lens, where the sample is positioned, which can be seen in Fig. 3.2. In order to decrease the focal length of the lens, this gap is kept small, in many cases it can be in the order of 4–5 mm, but there are instruments with much smaller ($\leq$ 2 mm) and larger ($\geq$ 10 mm) pole gaps.

The most straightforward way to place an SPM instrument inside a TEM is to miniaturize the SPM so that it fits inside the space available, that is, that the SPM is small enough to fit inside the typical dimensions of a conventional TEM specimen

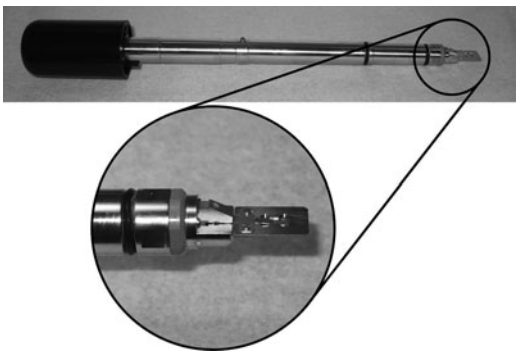

Fig. 3.1 Typical standard TEM specimen holder. In this case, the diameter of the shaft is approximately 18 mm, and the specimen support part is about 1 mm high

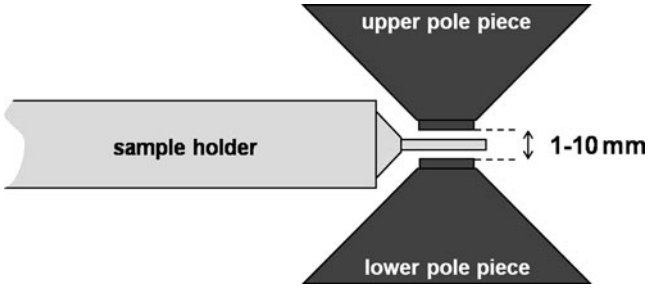

Fig. 3.2 Schematic of the upper and lower pole piece of the objective lens, with a sample holder inserted between the pole pieces

holder. The other approach is to modify the design of the TEM to accommodate a larger SPM device. The first approach has attracted the most interest because redesigning a TEM instrument is usually a complicated task. There are, however, a few examples of rebuilt TEMs in which an STM and an AFM have been incorporated [2, 21]. The different principles by which TEMSPM instruments have been constructed will be presented in this chapter.

3.3 Incorporating an STM Inside a TEM Instrument

The main challenge when incorporating an STM inside a TEM is the limited space available inside the pole-piece gap of the TEM. A traditional STM design is simply too large to be placed in a TEM, and in order to understand this challenge we first take a closer look at how the STM instrument has been developed. It began in the early 1970s when Young and co-workers envisioned an instrument, the "Topografiner," that would image a surface by sweeping a sharp tip over the surface at a constant, noncontacting distance [22]. In a method still practiced today, a tip is scanned over the surface in a raster pattern and by keeping the current constant the tip describes a trajectory that generates the surface topography. The current flowing in the tunneling mode is sensitive to the distance between tip and sample, which is of the order of only 1 nm. This puts very high demands on the mechanical stability of such an instrument. The mechanical stability was improved upon about a decade later by Binnig and Rohrer [23]. They dubbed their instrument a "scanning tunneling microscope" as it was, for the first time, able to acquire images in the tunneling mode and then display atomic resolution on semiconductor surfaces. Since then the mechanical stability and the controlling hardware and software have been improved even further.

To design an STM, a fine motion control of the tip (or sample) is required. This is usually performed by several piezo ceramic parts (or a single tube), giving the tip a movable range of a few micrometers in three dimensions. A coarse approach mechanism is also required to place the sample and tip in close proximity so that

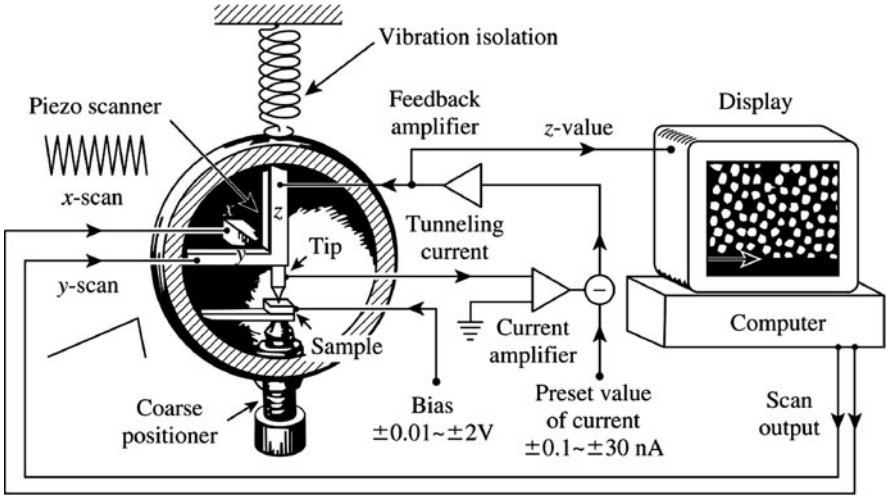

Fig. 3.3 Schematic drawing of the different parts that are needed for a complete STM system. Image is from [24]

the piezo motion is enough for the imaging. These parts should be kept small and sufficiently rigid to minimize the vibrational amplitudes of the tip in relation to the sample. A schematic drawing of the STM construction is shown in Fig. 3.3.

In connection to the development of the STM, there was also a desire to be able to "see" how these new instruments were actually operating. In 1986, Gerber et al. combined an STM with an SEM in order to study the STM in operation [25]. There were also ideas to use the STM and SEM in combination in order to extend the imaging capabilities of the fairly limited SEM instruments of the time 26]. To achieve a better resolution of the electron microscope part, an STM was fitted inside the sample holder of a TEM by Spence [27]. The tip and sample could be observed using the TEM in reflection mode (REM). The first studies were primarily aimed at monitoring the tip–sample interaction and to better understand how the STM operated and imaged a surface [28]. Detailed and valuable data were collected revealing tip changes during deliberate tip alterations as well as regular scanning [2, 29]. After the first STMs were incorporated into TEM instruments, it became apparent that the combined instrument was much more than a mere combination of two imaging methods. Instead, it can be considered to have movable, high precision, electrical probe available inside the imaging TEM. Applying this perspective extends the capabilities of the TEM beyond passive sample observation. The latest developments have indeed gone in that direction, and the modern TEMSTM systems are rarely used for actual STM imaging; instead they are used for sometimes very intricate manipulations and characterizations of complex nanostructured materials (see Sect. 3.3.1).

As mentioned earlier, the main challenge when combining STM and TEM is the limited space available within the pole-piece gap of a TEM. The most common

approach to fit an STM in a TEM is to custom make a side-entry holder that includes a coarse motion control and a fine piezo motion, all within the regular size of a sample holder, and thus no modifications to the TEM itself are needed. The first report of using such a configuration was by Spence [27], where a single piezo tube was placed inside a side-entry holder and driven back and forth by a linear motor. For that particular TEM, the pole gap was fairly large (9 mm) and the STM part was kept below 7 mm in diameter. The same design ideas have since then been used by others for more demanding pole pieces. The pole-piece gaps of high resolution instruments can be rather small and require holders with sub-millimeter thickness in the sample region. A one-dimensional coarse motion of the tip towards the sample can be realized by an inch worm [27,28,30], a micrometer screw [1,31], or a stepper motor [32]. In order to obtain a high mechanical stability, the linear drive can be decoupled from the piezo when the coarse motion is not needed.

An alternative approach worth mentioning here is a custom-made micro-STM instrument (μ-STM) presented by several groups [33,34], which consisted of micromachined silicon structures in order to build up a complete STM instrument in one single chip. A comb structure was used for the linear drive of the tip toward the sample and out-of-plane motion was achieved by torsional motion [34]. These instruments were fairly limited because there was no obvious way to incorporate traditional tip and sample materials. To our knowledge, the development of the μ-STM has not continued past these initial attempts.

More demanding applications have emerged when one wants to study electron transparent materials in electron transmission mode. The samples must be very thin (typically 20–300 nm), and the limited range of the piezo makes ex situ alignments rather impractical as the tip has to effectively find a knife edge inside the TEM. Ideally one should have full three-dimensional coarse motion of the tip (or sample) so that any part of the sample can be reached in situ. The first real attempts at full three-dimensional coarse motion were presented by Olin et al. [32]. In this approach, a coarse motion mechanism was fitted to the end of the piezo scanner tube, thus allowing full three-dimensional coarse and fine motion while maintaining atomic level resolution in both STM and TEM mode [35]. Figure 3.4 shows the TEM sample with this coarse motion incorporated. The coarse motion mechanism utilizes a tip holder connected to the piezo by six springs that clamp around a metal sphere. When the piezo is moved at typical scan speeds the tip holder with its low mass simply follows the motion of the piezo. When much faster, jerking, motions are performed by the piezo, the tip holder will slide against the sphere that is rigidly attached to piezo. In this way, the tip holder and the tip apex can be moved by coarse and fine motion in all three directions. The detailed construction of the springs limits the coarse motion to around 1 mm (in all three directions), which is enough to cover the typical sample area inside a TEM. The friction force is also large enough to allow physical manipulations of nanostructures with the tip, as these are generally in the μN range or lower, while the friction force of the tip holder is in the range of hundreds of mN [35]. This construction can be adapted to any side-entry TEM, and the instrument can be further customized on the fixed side to accommodate special samples, such as those with several electrodes. The fixed side could also contain a

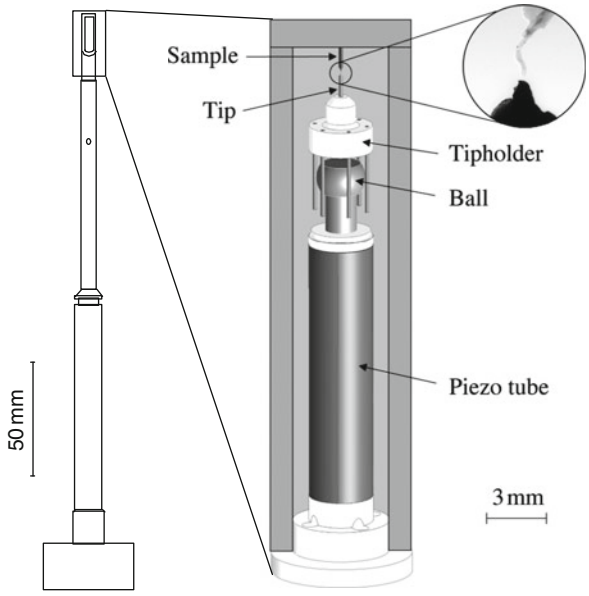

Fig. 3.4 Schematic illustration of the TEMSTM holder with the integrated three-dimensional coarse motion mechanism. The *inset* shows TEM image of sample and tip. Image is from [35]

force sensor, and thereby an AFM has essentially been joined with the TEM. This design forms the basis for commercial TEMSPM instruments [36].

3.3.1 Applications of TEMSTM

The earliest STM instrument inside a TEM by Spence et al. was mainly considered to be a complementary microscope for surface imaging [27, 37, 38]. Other early studies include the work by Takayanagi et al. on the interaction between a STM tip and a sample [2, 29]. Later it was realized that the real power was in the use of an STM tip for local probing of electrical properties and manipulation of a sample.

3.3.1.1 Electron Transport Studies

In one of the first studies when using the TEMSTM as a probe instead of as an additional microscope, Takayanagi et al. used the STM tip both for forming atomic-sized gold wires and measuring the conductance of these wires [39]. By pressing two gold tips together and then retracting them, a nanosized wire was formed before rupture. The entire process of nanowire formation was imaged by TEM and correlated simultaneously with electrical measurements. The thinnest wires were only one atom

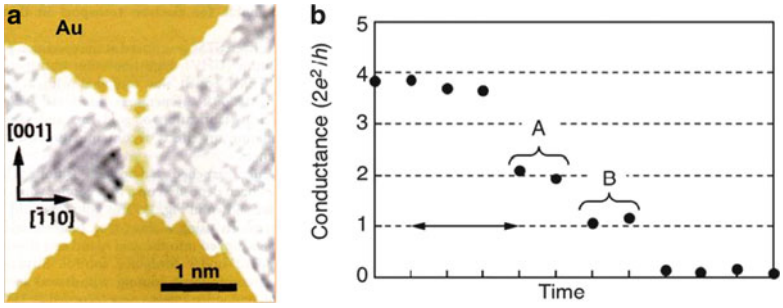

Fig. 3.5 Quantized conductance of atomic-sized gold wires studied by TEMSTM. (**a**) TEM image of a wire consisting of four gold atoms. (**b**) The corresponding conductance measurement, in units of $G_0 = 2e^2/h \sim (13\,\mathrm{k\Omega})^{-1}$, while withdrawing the tip. Images are from [39]

wide, as can be seen in Fig. 3.5. In such small conductors, the electron transport is ballistic and the conductance is quantized in units of $2e^2/h \sim (13\,\mathrm{k\Omega})^{-1}$, where e is the electron charge and h the Planck's constant. These studies were done to answer the open question about the microstructure of earlier observations of quantized conductance in similar ex situ STM experiments (for a review see [40]). The work by Takayanagi et al. solved this problem and gave direct evidence of the structure of these atomic sized conductors [41–43]. However, there were also new surprises, such as the anomalously long distance between the atoms in the wire.

Using the same kind of pressing-retraction method, Erts et al. studied larger point contacts of gold nanowires ranging from atomic size to 20 nm in diameter [44]. For the smallest ones, the electron transport was ballistic, but for the larger ones the transport became more and more diffusive. The degree of diffusive electron transport was determined by using the TEM to measure the radius and the STM for contact formation and conductance measurements. The electron mean free path was found to be ten times shorter than the bulk value. This indicates that the earlier calculation of the radius of the point contacts from conductance measurements is misleading by an order of magnitude.

With the increasing interest in carbon nanotubes there have been numerous investigations of their electrical properties [45, 46]. Multiwall carbon nanotubes, concentrically stacked tubular sheets of graphite, were extended in a telescopic manner using an STM probe and their nonlinear electrical resistance change was monitored [47]. In this type of study it is important to have proper electrical contacts, as will be discussed in Sect. 3.5. For example, in an early study by Frank et al. [48], the electron transport of carbon nanotubes was determined by dipping the nanotube in a drop of mercury. With this contacting technique, ballistic conduction was suggested; however, it is not without problems. Recently, it has been demonstrated that the nanowire does not actually enter the mercury droplet due to the high surface tension and a formation of a skin on the mercury surface [49]. This behavior gives a conductivity that appears to be independent of the distance between the electrodes, while in fact the distance remains the same during the dipping process.

Also, other materials such as III–V semiconductors, such as InAs, have been electrically characterized [50] using TEMSTM. The advantage of the TEMSTM method is the correlation between the microstructure determined by TEM imaging and analysis and the direct electrical measurement, but also the simple way to select and contact single nanowires. A challenge for the future is to provide a method to extend this two-probe method to permit four-point measurement in order to avoid the often unknown contact resistance.

3.3.1.2 Field Emission

In situ TEM probing of field emission was first studied by Wang et al. [6, 7, 31] and Kuzumaki et al. [51–53], which revealed the structural change of the electron emitting carbon nanotubes. Cumings et al. [54] performed electron holography of field-emitting carbon nanotubes to determine the magnitude and spatial distribution of the electric field surrounding the tubes. Sveningsson et al. [5] measured the electron emission from carbon nanotubes and observed that for low currents the emission was of a standard Fowler–Nordheim type, while for higher emission currents a nonlinear behavior occurred due to thermally enhanced emission caused by Joule heating of the carbon nanotube. A detailed study of the correlation of the structure of carbon nanotubes and electron emission as well as the structural change during emission was done by Wang et al. [55]. An interesting combination of the resonance method to determine the work function [56, 57] and field emission was done by Xu et al. [58]. In the Fowler–Nordheim model, the field emission current is determined by two factors, the field enhancement factor β and the work function ϕ, and the emission current is

$$I = KF^2 / \phi \exp(-B\phi^{3/2} / F), \tag{3.1}$$

where $B = 6.83 \times 10^9$ V eV$^{3/2}$ m^{-1} and K is a constant. The local electric field F is related to the applied voltage V as $F = \beta V/d$, where d is the distance between the electrodes, as seen in Fig. 3.6. The standard way to determine β from measurements is to use a Fowler–Nordheim plot, $\ln(I/V^2)$ vs. $1/V$ (Fig. 3.6), and from the plot the slope $(-B\phi^{3/2}d/\beta)$ is determined. If the work function is known, the field enhancement factor can then be calculated. The work function is sensitive to small changes of the emitting nanotube; however, by using the TEMSTM in the mechanical resonance mode, the work function could be measured in the same setup. In another combined mechanical resonance-field emission study, Xu et al. [59] showed how the field emission current had a periodic oscillation component with a frequency that was twice the mechanical resonance frequency.

3.3.1.3 Electromigration

Svensson et al. studied the electromigration of iron particles inside carbon nanotubes [60]. Above a critical current density of 7×10^6 A cm^{-2} the iron particles started

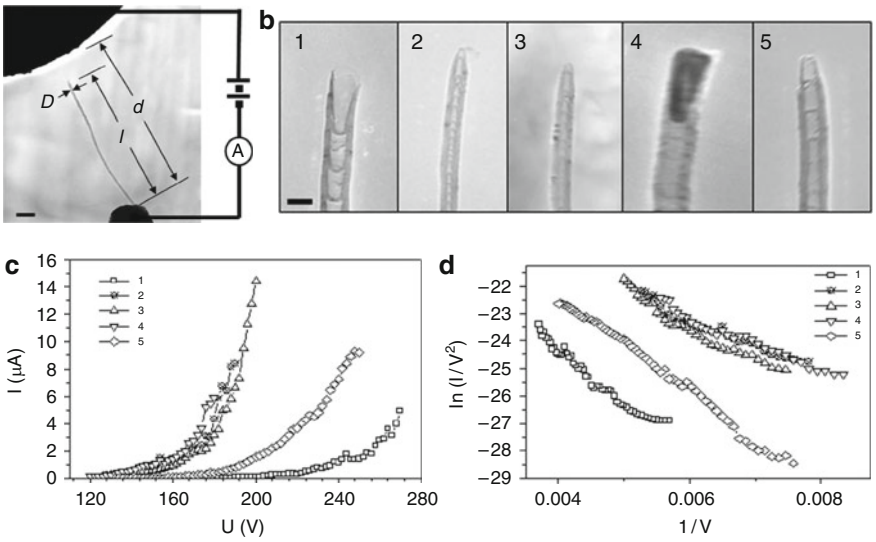

Fig. 3.6 TEMSTM study of field emission from carbon nanotubes. (**a**) TEM image of the nanotube and the electrodes with geometrical definitions. *Scale bar* is 200 nm. (**b**) TEM images of the microstructure of the emitting part of the carbon nanotubes. *Scale bar* is 50 nm. (**c**) Current–voltage curves for the different nanotubes. (**d**) The corresponding Fowler–Nordheim plot. Images are from [58]

to migrate in the same direction as the electron current. The "wind" of the electrons transfers a moment to the particles, which is known as electromigration (see Fig. 3.7h–k). In the same study, these effects were used as a kind of nanopipette to reversibly eject, deposit, and retrieve the iron particles from the end of the carbon nanotube, as shown in Fig. 3.7a–g. Electromigration has been used in several studies; for example, for transport of indium particles on the surface of carbon nanotubes [61], for welding carbon nanotubes [62], for mass transport through the walls of carbon nanotube [63], for transport of CuI particles in carbon nanotubes [64], and in applications for archival memory devices [65].

3.3.1.4 Joule Heating

A high current through a nanowire or nanotube could lead to resistive heating, called Joule heating. This current, I, will inject a heating power, P, of I^2R, where R is the resistance of the nanowire. The heat will lead to an increase in temperature that can easily reach the melting point of the material. Joule heating can be used to anneal samples, evaporate some of the material in a wire, or to decompose compounds. Joule heating is also, for example, used for welding materials together or removing contaminations.

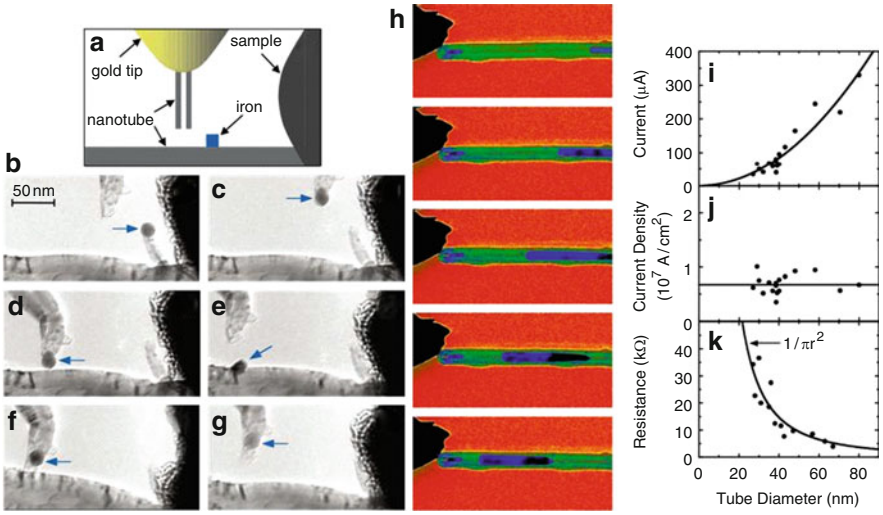

Fig. 3.7 Electromigration experiments using the TEMSTM. (**a–f**) Sequential TEM images demonstrating the nanopipette action. The transferred iron is indicated by an *arrow*. (**a**) Schematic drawing of the setup. (**b**) Iron has been migrated to the end of a fixed nanotube. (**c**) Iron is retrieved using a nanotube attached to the movable tip. (**d**) The nanotube is directed at the side of a large nanotube. (**e**) The iron is deposited. (**f**) The iron particle can be retrieved again. (**g**) The iron particle is ready to be deposited elsewhere. (**h**) Electromigration of an iron particle inside a carbon nanotube. (**i–k**) Electrical data measured on iron-containing carbon nanotubes as a function of diameter. (**j**) The iron particle starts to move above a certain critical current density. (**k**) The resistance measurement also shows that the electron transport is diffusive, because the resistance is inversely proportional to the cross-sectional area. Images are from [60]

Annealing and Evaporation

Annealing by in situ Joule heating on carbon nanostructures has been performed by Huang and co-workers, for example, on the crystallization of amorphous carbon (a-C) into carbon nanotubes [66] with a resulting increase in electrical conductivity [67]. The elevated temperature also allows super plastic deformation of the carbon nanotubes [68], that is, when the material is deformed well beyond its usual breaking point, usually exceeding 100% during tensile deformation. Such a super plastic state is achieved at a high temperature, typically at half the melting temperature. Increasing the electric power beyond that point will instead lead to breakdown of the nanotube [69], unless, as shown by Zettl et al., a controlled application of Joule heating, electromigration, and electron beam irradiation could reduce the diameter of a carbon nanotube, shrinking the tube from several nanometers down to near zero [70]. In situ Joule heating is also used to study other forms of carbon and graphene sublimation, and multilayer edge reconstruction has been observed [71] in such processes.

The structural variation of a-C nanocontacts during voltage application was observed while simultaneously measuring the I–V characteristics of a-C nanocontact

[72]. The maximum current density and resistivity of a-C nanocontacts were 2.8×10^{11} A m^{-2} and 8.5×10^{-3} Ωm, respectively, at a bias voltage of 2.3 V. When the voltage was reduced below 1.4 V, the current was maintained at zero and during this voltage reduction, the a-C nanocontacts transformed into graphitic nanocontacts with a thickness of 2–3 atomic layers. The observation presented in [72] shows that stable graphitic nanocontact is obtained when the first voltage applied.

Decomposition

Decomposition of compound materials has also been studied using in situ TEM Joule heating, for example, in the form of GaN nanowires [73] and BN nanotubes [74, 75]. Both the GaN nanowires and the BN nanotubes show thermal decomposition by leaving nanoparticles (Ga in the first case and B in the second) behind on the surface of the nanowires before failure. In another study of a compound nanowire, both the decomposition and the annealing phases were observed [76]. $Mo_6S_3I_6$ decomposed to metallic Mo below 1,000°C, when the S and I atoms evaporated. The annealing process of the remaining Mo nanowires revealed details about grain growth and the increased conductivity due to a lower degree of scattering, as seen in Fig. 3.8 [76].

Growth

Joule heating can also be used for growing structures inside a TEM. For example, carbon nanotubes [77] and carbon fullerenes have been grown in the gap between two gold electrodes [78]. By depositing gold nanoparticles on carbon nanotubes and using Joule heating of the carbon nanotube, it is possible to grow carbon nanocages using the gold nanoparticles as templates [79]. By increasing the temperature with Joule heating, the gold nanoparticles were evaporated leaving the empty carbon cages behind. In a similar study, a-C was Joule heated, and by using platinum particles as templates, 1–5 graphite layer thick cages were grown [80]. In another study, the TEMSTM and electron beam induced deposition (EBID), a-C nanowires were grown and graphitized mediated by iron particles [81].

Welding

Another application of Joule heating is in the welding of nanostructures, for example, interconnections of nanobuilding blocks, such as carbon nanotubes, nanowires, nanobelts, nanohelixes, and other structures for the assembly of nanoelectronics or nanoelectromechanical systems (NEMS). Compared to other interconnection processes, electrical spot welding has several interesting aspects: (a) a low electron current can induce melting more efficiently than irradiation-based techniques involving high electron beams, focused ion beams (FIB), or lasers; (b) the welding site can readily be selected by using a three-dimensional positioning and

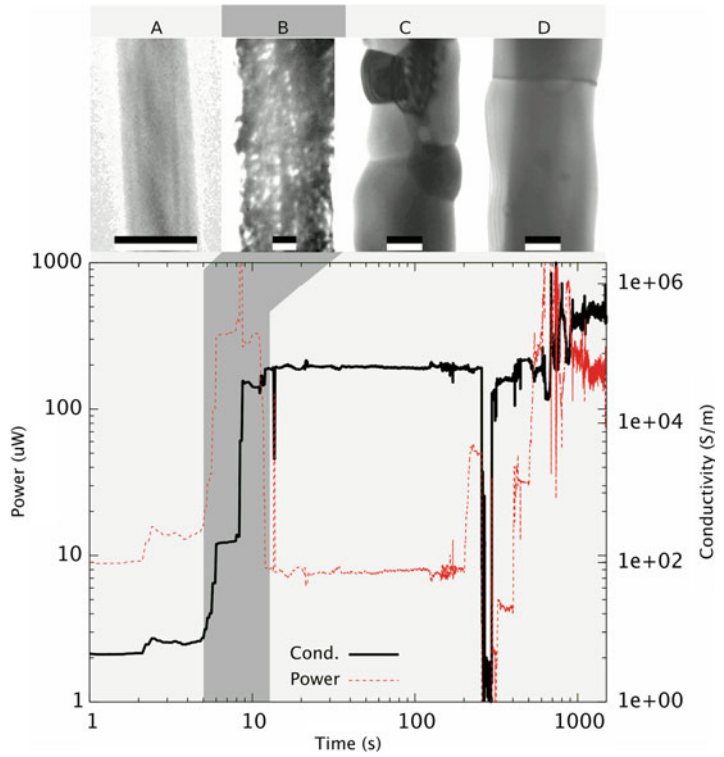

Fig. 3.8 Joule heating of a compound nanowire, $Mo_6S_3I_6$, demonstrating both decomposition and annealing. (**a**) A fresh sample $Mo_6S_3I_6$ is shown. (**b**) The $Mo_6S_3I_6$ nanowire has decomposed and only Mo remains. (**c**) The nanowire is annealed. (**d**) The nanowire wire after further annealing. Note that the TEM images are from different nanowires. The *scale bars* are 100 nm in (**a**) and 50 nm in (**b–d**). Images are from [76]

manipulation probe, which may potentially enable three-dimensional prototyping and assembling; (c) the melting process is very fast, compared with, for example, high intensity electron beam or FIB. Nelson et al. have reviewed several aspects of nanospot welding [11–13].

In the early study by Hirayama et al., bundles of single-wall nanotubes (SWNT) were spot welded together [82]. At a voltage of 2 V and a current of 20 nA, which gives an injected power of 40 nW, the bundles adhered to each other permanently. This was interpreted as spot welding of the tubes by Joule heating.

Spot welding using single crystalline copper filled carbon nanotubes was investigated by Dong et al. [62]. Controlled melting and flowing of copper inside nanotube shells was realized by applying a bias voltage between 1.5 and 2.5 V. The melting was a result of Joule heating, while the flowing was caused by electromigration, where the latter occurred at a critical current density of 3×10^6 A cm^{-2}. The flow rate of the copper was approximately 10 nm s^{-1} at 2.5 V bias, which allowed precise control of the mass transport.

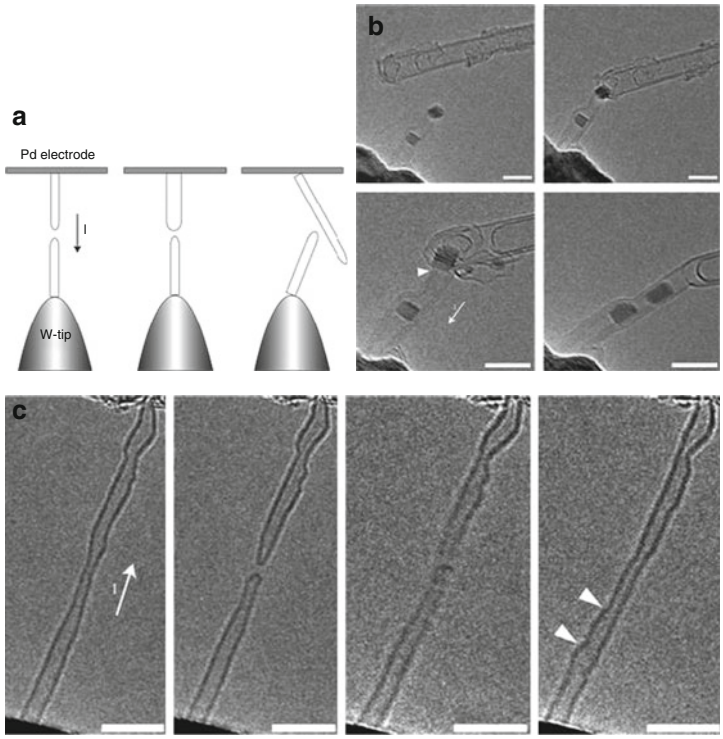

Fig. 3.9 Joining carbon nanotubes with Joule heating. (**a**) A schematic of three typical geometries joined. (**b**) Joining two nanotubes with different diameters using a tungsten particle. The *scale bars* are 5 nm. (**c**) Breaking and joining SWNTs. The *scale bars* are 5 nm. Images are from [83]

Jin et al. [83] reported on a similar welding process of Joule heating to seamlessly join two carbon nanotubes of similar diameter to form new carbon nanotube structures. With the assistance of tungsten particles, carbon nanotubes of different diameters could be joined, as seen in Fig. 3.9b. To join two SWNTs with identical diameters, the nanotubes were first broken into two parts using an electrical breakdown process. The two resulting capped SWNTs could be mechanically recontacted by moving the SWNT mounted on a tungsten wire on the STM probe in close proximity to the second SWNT mounted on a counter electrode. The voltage and current were raised from zero, and by passing threshold voltages, the SWNT joined again into one carbon nanotube. This process of breaking and joining could be repeated up to seven times. Images from these procedures are seen in Fig. 3.9.

Another form of welding, not related to Joule heating, is based on EBID of a-C. This welding process was used by Wang et al. to fix bended carbon nanotubes into a desired morphology [84]. The freestanding nanotubes were bent by an STM probe and then fixed by the deposition of a-C onto the bent area. The mechanical strength of the bent carbon nanotube may be greatly enhanced by increasing the amount of a-C on the deposition area. The electrical conduction of the nanotube has been

observed to be independent from the bending deformation and the deposition of a-C. Furthermore, metals such as tungsten, gold, and platinum can be deposited on carbon nanotubes. Using the EBID process, an organometallic compound can be decomposed to fix the bent carbon nanotubes or even connect them to each other [85] and to mount them on a substrate [86]. The disadvantage of using metals is that metal particles can be melted, vaporized, or moved along the carbon nanotubes by Joule heating and electromigration. Also, there is a substantial amount of organic residues left from the EBID process that might be of consequence if a low ohmic contact is needed.

3.3.1.5 Mechanical Studies

Even though the TEMSTM is an electrical probe, there are several ways that it can be used to analyze mechanical properties. For example, Poncharal et al. [7,31,87,88] applied an alternating electric field between an STM tip and a separated carbon nanotube which made the nanotube vibrate. By increasing the frequency of the alternating voltage, the nanotube will reach its resonance frequency as observed by TEM imaging, as shown in Fig. 3.10. The TEM images give information about size, and along with the information about the resonance frequency, the elastic modulus can be calculated from the Euler–Bernoulli beam equation:

$$f_n = \frac{\beta_n^2 D}{8\pi L^2}\sqrt{\frac{E_\mathrm{b}}{\rho}}, \tag{3.2}$$

where f is the frequency, β_n are constants for the nth harmonic: $\beta_1 = 1.875,\ \beta_2 = 4.694,\ L$ is the length, D is the diameter, ρ is the density, and E_b is the effective

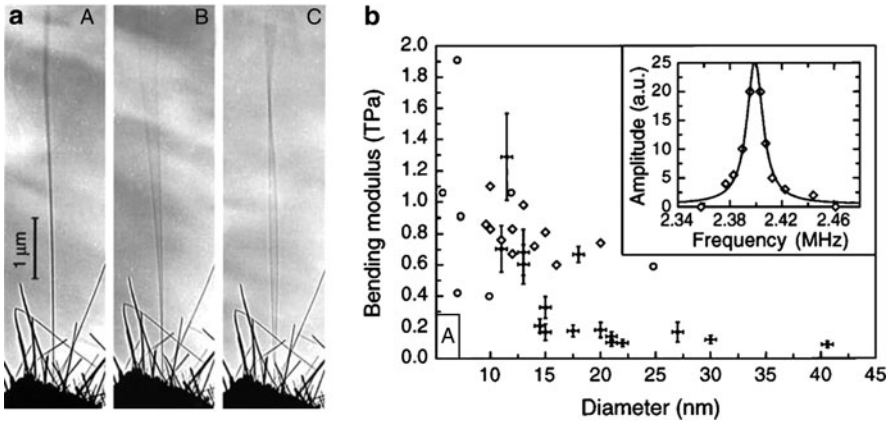

Fig. 3.10 (**a**) The TEM image shows how carbon nanotubes were excited using the TEMSTM. (**b**) The resonance frequency and bending modulus measured. Images are from [87]

bending modulus. From the same kind of measurement, the damping or Q-value can be deduced from the amplitude change around the resonance frequency. High elastic modulus values are expected for carbon nanotubes, for carbon nanotubes with diameters below 5 nm, there have been reports on elastic modulus values up to 1 TPa, comparable to diamond. The mechanical resonance could also be induced by thermal energy and this is visible for long and weak nanowires and nanotubes [89] By comparing the thermal energy, $k_B T$, with the mechanical energy (kA^2, where k is the spring constant and A the amplitude of the vibrating tube), the thermally induced vibrations can be calculated. For a long and thin nanotube or nanowire the spring constant will be low, making this effect readily visible in the TEM as a blur of the nanotube image.

The work function of nanosized materials can also be measured using a variant of the resonance method [56, 57] in a way similar to the Kelvin probe method. In this technique, the resonance frequency is first found as described above, and then by adding a static voltage V_{dc} to the alternating voltage V_{ac}, the amplitude of the oscillating nanowire will change. It can be shown that when V_{dc} is equal to the difference in work function between the nanowire and the counter electrode, the mechanical amplitude will be zero. A false signal could be observed if a high V_{dc} (around several volts) is applied when the distance between the electrodes is short. The oscillating nanowire will be under tension from the electrostatic field, and like tuning the resonance frequency of a spring by applying tension, the resonance frequency will shift away leading to lower amplitudes. This technique was used to determine the work function of carbon nanotubes that were either 0.3 eV below or 0.6 eV above graphite. This measurement was interpreted as the identification of metallic and semiconducting carbon nanotubes [57].

Several other mechanical studies using TEMSTM have been done, including linear bearings in the form of carbon nanotubes sliding inside each other [90], contact formation between gold wires [91], or even NEMS devices in the form of a nanorelay consisting of Ge or Si nanowires [92, 93] or $Mo_6S_3I_6$ nanowires [94].

3.4 Incorporating an AFM Inside a TEM Instrument

The atomic force microscope (AFM) was introduced by Binnig et al. [95] in 1986 as a continuation of the STM. Instead of tunneling currents, the AFM utilizes forces between surfaces to generate an image of the topography; thus, the AFM is not restricted to imaging conductive materials but is also capable of resolving features on an atomic scale for nonconductors. There are two main imaging modes available in the AFM, contact and noncontact mode. In contact mode, the AFM tip is in contact with the sample during imaging and in noncontact mode the AFM tip is excited to its resonance frequency and scanned along the surface at a close proximity.

As the AFM technique was developed, there was a desire to perform advanced mechanical characterizations by utilizing the AFM as a local force probe on, for

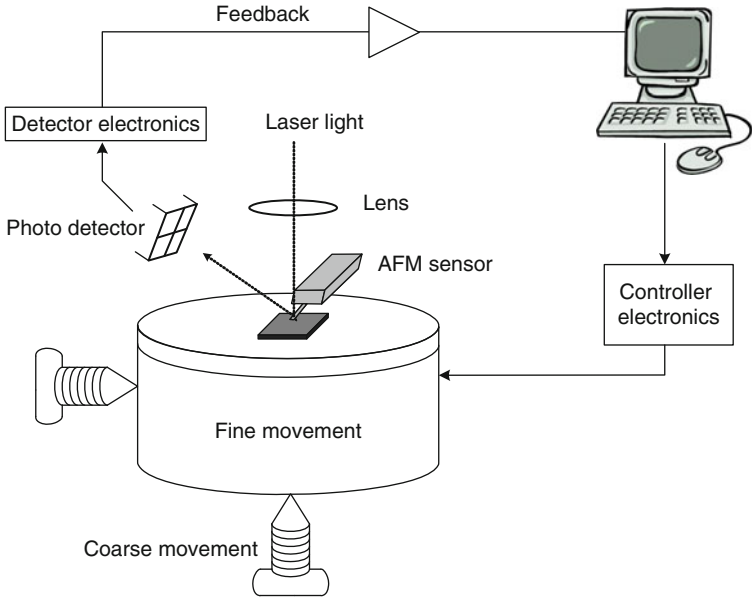

Fig. 3.11 Schematic of a standard atomic force microscope with an optical deflection detection system

example, nanowires. To do this, simultaneous imaging is needed. To enable such experiments, the AFM was first combined with the SEM [96, 97] in 1994 and for higher imaging resolution with the TEM [3, 21] in 2001. The high imaging resolution of the TEMAFM enables measurements on nanostructures such as nanowires and nanoparticles, opening up new possibilities in nanoscale mechanical characterization.

As mentioned previously, the main challenge of a TEMAFM instrument is to fit an AFM inside the TEM pole-piece gap, as illustrated in Fig. 3.1b. A standard AFM system consists of a coarse and fine motion to align the sample and tip, and a system to measure the deflection of the tip in order to be able to control the applied force. In standard AFMs, an optical system for detection of the deflection is the most common configuration. A sketch of a standard AFM system is shown in Fig. 3.11. To construct a TEMAFM instrument, all of these components need to be fitted in the TEM pole-gap.

3.4.1 Optical Force Detection Systems

One of the first TEMAFM systems was presented by Kizuka et al. [21] in 2001. In this work, a HRTEM was rebuilt to incorporate an AFM and an STM. The coarse motion in this system was realized using the positioning stage of the TEM, the

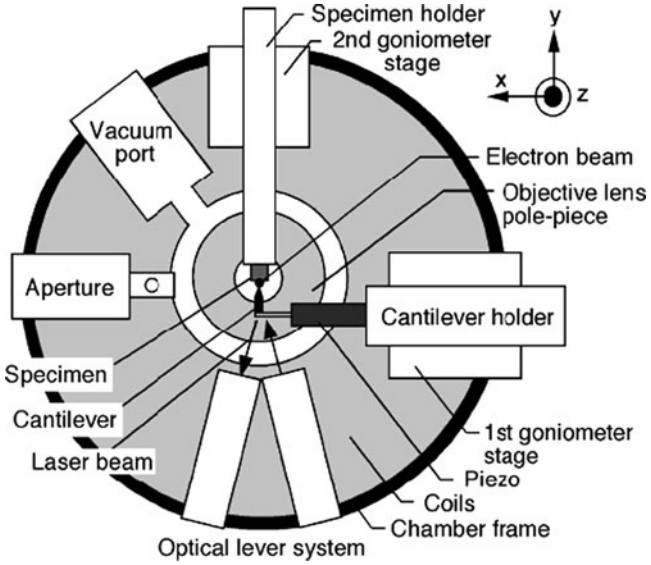

Fig. 3.12 A cross section of the TEM column showing modifications to facilitate an AFM system with laser detection system as presented in [21]. Image is from [21]

goniometer. In [21], the TEM was rebuilt to include two goniometer stages, where the sample is mounted on one stage with an AFM sensor, and a piezoelectric actuator on the other, as shown in Fig. 3.12. To perform an experiment, the two goniometers are used to align the sample and tip, while the piezoelectric actuator (on which the AFM sensor is mounted) is used for high precision movement. The deflection of the cantilever, and consequently the force, is measured using an optical detection system built into the TEM column.

The TEMAFM instrument presented by Kizuka and co-workers is the only known example in which a TEM has been extensively redesigned to fit an AFM. The two main reasons it has not been done previously are the significant cost related to rebuilding a TEM and the extensive collaboration with a TEM manufacturer that is required. Other approaches to implement a TEMAFM for which the TEM does not need to be redesigned have attracted more attention.

3.4.2 Non-optical Force Detection Systems

Simple Spring Approach

The simplest way to measure forces inside a TEM is to use a spring with a known force constant and then image the deflection of the spring using the TEM.

Practically, this is done by placing a standard AFM cantilever at the fixed position in a TEMSTM holder described in Sect. 3.3. Such a configuration was presented by Erts et al. [3] in 2001.This scheme eliminates the extra space needed for an optical deflection detection system, and by placing the AFM sensor on the fixed side, additional inaccuracies in the force caused by the characteristics of the fine movement, that is, the piezo, were avoided. The AFM cantilever was used as a mechanical spring, for which the spring constant is known. The force was extracted using Hooke's law, $F = -kd$, where k is the spring constant of the cantilever, d is the deflection of the cantilever, and F is the force. This configuration has been used to study the mechanical properties of single carbon nanotubes [51–53, 98], welded gold nanowires [99], and the initial contact and adhesion forces in a gold nanocontact [100]. Figure 3.13 shows TEM images of a gold nanocontact experiment and the force measured [100]. The gold nanocontact was created by bringing a gold coated AFM tip into contact with a gold wire and then retracting the tip from the wire.

This technique is straightforward to use when the TEM holder used is equipped with a positioning system, as it does not require any reconstruction other than mounting of an AFM cantilever. It is possible to perform mechanical characterization; however, for more advanced analyses, the technique is limited by two main factors. First, the sampling rate will be low, as seen in Fig. 3.13b. Because the procedure is done manually, every force point is calculated from the cantilever deflection, which in turn is extracted from a comparison of TEM images captured during the experiment. Second, with this technique the force range is limited by the image magnification because the deflection must be visible in the image. As a result of these limitations, a compact force measurement system not reliant on the TEM imaging is desired.

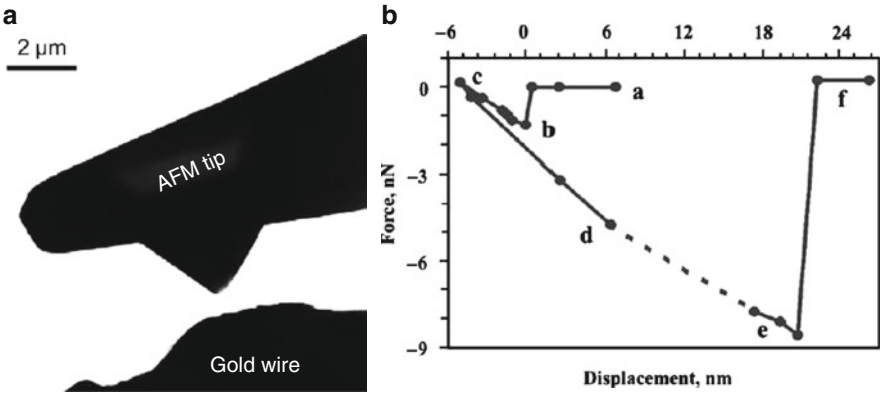

Fig. 3.13 TEMAFM measurement in which two gold surfaces were brought in contact and retracted to study the surface interaction. (**a**) Low magnification TEM image of the gold coated AFM tip and the gold wire. (**b**) The force–distance curve when retracting the gold surfaces from each other. Images are from [100]

Electrical Force Sensors

In order to enable direct force measurement without redesigning the TEM column, a compact electrical AFM sensor in combination with a miniaturized positioning system is needed. Different force detection techniques have been developed for standard AFMs, including current tunneling [95] optical interferometery [101, 102] and electrical techniques such as capacitive [103, 104], piezoelectric [105], and piezoresistive [106] techniques. For in situ TEM instrumentation, capacitive force detection has been used for measuring forces in the μN range utilizing MEMS devices [107,108] and a miniaturized capacitive transducer based on [109]. Thus far, for in situ TEMAFM, which measures forces in the nN range, only piezoresistive detection has been utilized. The detection sensor, presented by Nafari et al. [110], was custom designed to fit inside a Phillips CM200. In that system, the dimensions of the sensor were chosen such that firstly, the sensor fits in the TEM pole-piece gap, and secondly, the sensor tip is centered in the TEM holder aligned to the electron beam. Considering these factors, the final dimensions of the sensor were restricted to 1.3 mm × 1.2 mm × 0.5 mm. The critical dimension is the width of the sensor (1.2 mm) as it will be mounted on the side of the holder so that it will not block the electron beam. The AFM tip is created in the fabrication process as an integral part of the sensor and is made of single crystalline silicon. The arrangement of the sensor and positioning system is shown in Fig. 3.14. This sensor has been integrated in a TEMAFM system, available commercially [36].

The resistors on this sensor chip were assembled in a Wheatstone bridge configuration integrated on the sensor chip as shown in Fig. 3.15. One of the resistors was doped into a reference cantilever (R_2 in Fig. 3.15a) for temperature compensation, which is especially important when operating in vacuum. This type of temperature compensation is described in detail by Thaysen et al. [111].

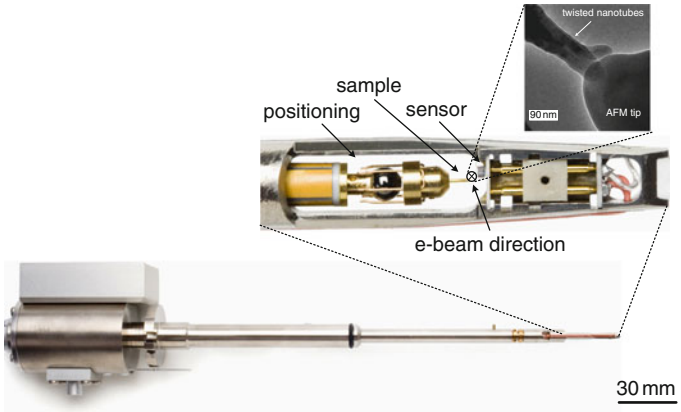

Fig. 3.14 Side view image of the TEMAFM system presented by Nafari et al. [110]

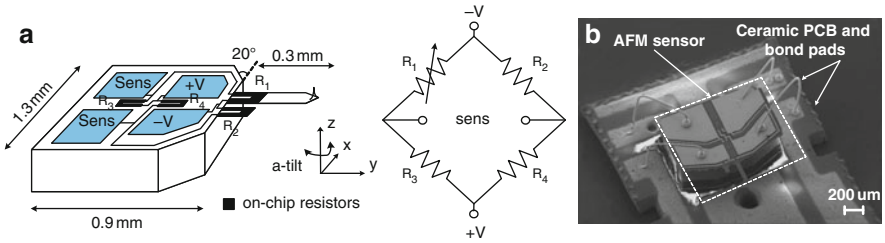

Fig. 3.15 The TEMAFM sensor presented in [110]. (**a**) The TEMAFM sensor design with the Wheatstone bridge configuration on chip. (**b**) SEM image of the TEMAFM sensor. Images are from [110]

3.4.3 TEMAFM Applications

While the TEMSTM was first used as an additional microscope, the TEMAFM that was introduced later was directly used as a local probe, with the TEM as a guide for locating suitable samples and for sample–tip characterization. As a local force probe, the TEMAFM has been a useful tool for studying the mechanical properties of individual nanostructures, friction at the nanoscale, and force interactions in nano and atomic sized contacts.

3.4.3.1 Elastic Measurements

A direct application of the TEMAFM is to study the elastic properties of nanostructures, such as nanowires and nanoparticles. There are several important issues related to the elastic properties of nanowires and nanotubes. The record high elastic modulus of carbon nanotubes of up to 1 TPa, as earlier observed by the TEMSTM method, raised questions of the elasticity of other nanostructures. The mechanical properties, including the elastic modulus and damping, are the key parameters in designing NEMS devices. The TEMSTM has been used to address these issues by the resonance method as described in Sect. 3.3.1, but a more direct way is to utilize the TEMAFM with its ability to measure nN forces during bending of a nanowire and to use the TEM for imaging of the nanowire size and shape. These structures are challenging to measure using a standard AFM because the AFM cannot be used for both imaging and point force measurements simultaneously, and the sample requires an elaborate preparation [9].

The TEMAFM characterization of nanostructures is generally performed by first attaching the nanostructures to a wire, typically using electrically conductive glue, and then mounting it in the sample holder. With the sample in place and inserted into the TEM, the nanowire is aligned to the AFM tip and a force can be applied. For example, in a study presented by Golberg et al. [112], the TEMAFM was used to investigate the elastic deformation of multiwalled BN nanotubes using the electrical force sensing TEMAFM system described in Sect. 3.4. Single-BN nanotubes were compressed, and it was found that they were elastic up

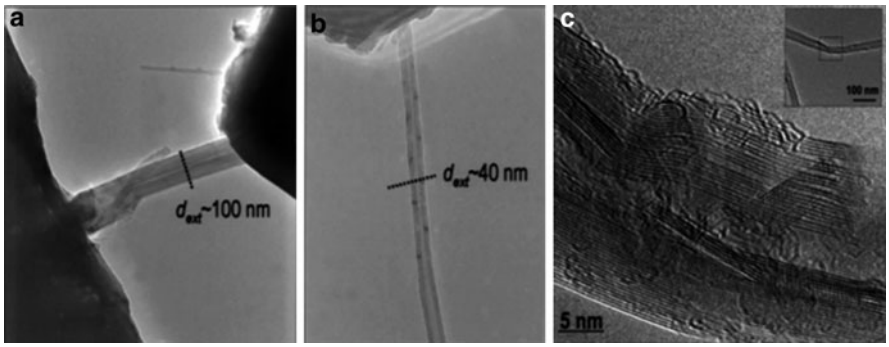

Fig. 3.16 TEMAFM elasticity study of BN nanotube. (**a**) A TEM image of the AFM tip, seen to the *right* in the image, connected to a BN nanotube. (**b**) A TEM image of a thinner BN nanotube connected to an AFM cantilever. (**c**) A high resolution image of the deformed layers in the multiwire structure. The images are from [112]

to a kinking of 90°, and the deformed layers after that point were studied, as shown in Fig. 3.16. By using the dimensions of the structures from TEM imaging and the measured force–displacement curves, a Young's modulus of 0.5–0.6 TPa was estimated for the BN nanotubes. The TEMAFM method has been used for a number of materials such as ZnO nanobelts [113], ZnO nanowires [114], TiO_2 nanotubes [115], carbon nanotubes [116–118], carbon nanocages [119–121], and C60 fullerene nanowhiskers [122, 123]. Golberg et al. have recently published a review of their TEMAFM work, summarizing the possibilities and challenges of the TEMAFM technique [10].

3.4.3.2 Electromechanical Properties

To investigate the electromechanical properties of nanostructures, a dual usage of TEMSTM and TEMAFM has been explored. In an experiment by Wang et al. [124] in 2009, the TEMSTM was used to modify cobalt-filled carbon nanotubes by driving a current through the nanotubes. Depending on the strength of the current, the cobalt particle was used to cut, repair, and interconnect carbon nanotubes with high precision. After the carbon nanotubes had been modified, the TEMAFM system was utilized to assess the mechanical properties. Figure 3.17 shows TEM images from this experiment. This technology opens the possibility to freely engineer advanced nanowire networks. Furthermore, in the work of Lu et al. [99] in 2010, the TEMAFM and the TEMSTM were used, separately, to investigate the properties of welded gold nanowires. With the help of in situ TEM techniques, it was shown that welding at the nanoscale was possible by simply joining two single-crystalline gold nanowires at relatively low pressure. TEM images and in situ probing showed that the welds were nearly perfect, with the same strength and conductivity as the rest of the wire.

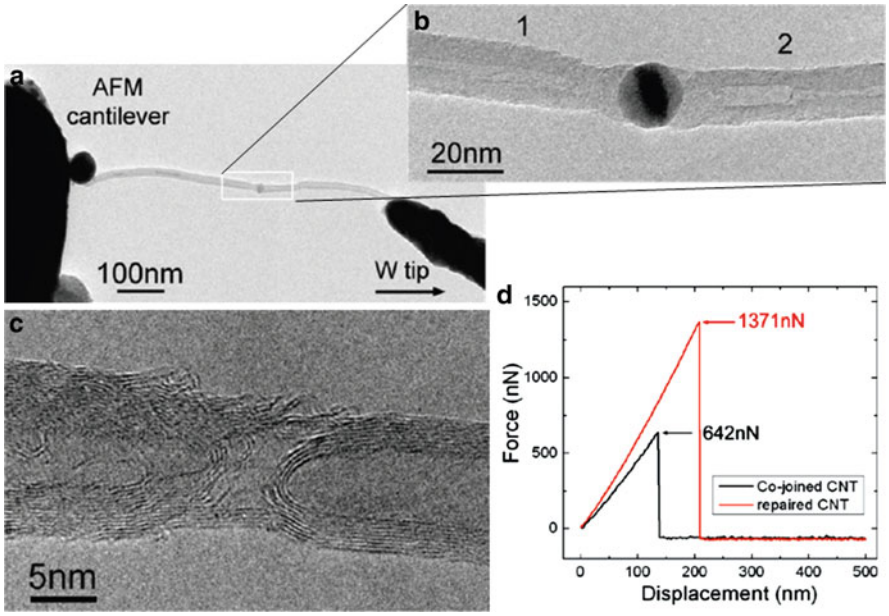

Fig. 3.17 TEMAFM measurement of welding of cobalt filled carbon nanotubes. (**a**) A carbon nanotube suspended by the AFM cantilever and a tungsten tip. (**b**) A zoom-in of the cobalt particle. (**c**) The carbon nanotubes joined without a cobalt particle. (**d**) The mechanical strength of a cobalt joined carbon nanotube and a repaired carbon nanotube. The images are from [124]

In a further development of the TEMAFM technique, an AFM sensor that allows simultaneous current measurements has been presented [36]. This conductive TEMAFM was used in the work of Costa et al. [125] to characterize the electromechanical properties of carbon nanotubes with crystalline fillings. It was shown that the filling dominated the mechanical properties of the carbon nanotube, and through electrical measurements, the semiconducting behavior of the filled carbon nanotube was observed simultaneously.

3.4.3.3 Atomic Scale Wires

The study by Takayangi et al. [39] on the correlation between the structure and the conductance quantization of atomic sized nanowires using the TEMSTM described in the Sect. 3.3.1.1 solved the open question regarding the structure of these small conductors. However, there were surprises in the study made by Takayanagi et al. [39], such as the anomalously long distance between the gold atoms. In addition, both theoretical [126] and experimental works using standard AFM [127] showed a correlation between the conductance and the tensile force; whenever the conductance changed one quantum unit ($2e^2/h$), the force made a jump of about 1 nN (for a review see [40]).

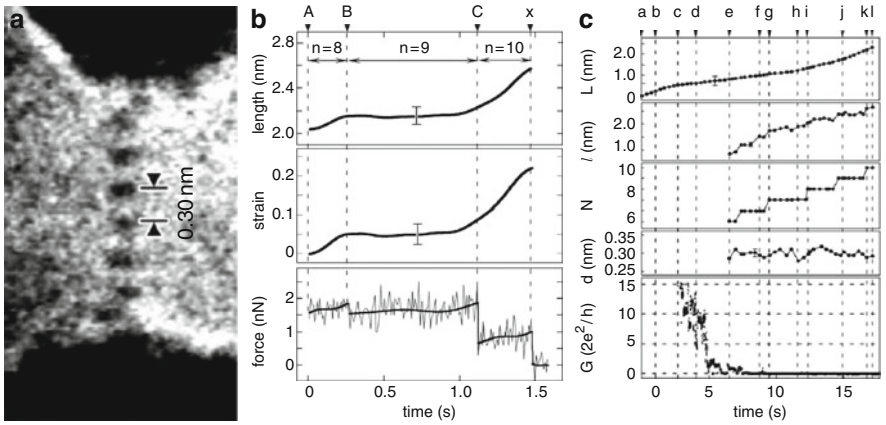

Fig. 3.18 TEMAFM study of single atom wide gold wires. (**a**) A single atomic wire created by separating two gold electrodes is seen. An interatomic distance of 0.3 Å can be measured from the image. (**b**) The force, strain, and length of the wires are seen as the number of atoms in the chain goes from eight to ten. (**c**) Conduction measurement while increasing the separation distance of the tip and plate. L is the separation distance, l is the total length of the atomic wire, N is the number of atoms, d is the interatomic distance, and G is the conductance of the wire during the tensile deformation. The images are from [124]

The TEMAFM might be a good tool to provide further insight into these problems. In a study by Kizuka, such an experiment was done on atomic sized gold nanowires [128]. Kizuka found several new surprises; for example, for ten atoms long wires a decrease in conductivity was observed, while for wires shorter than five atoms an increase was seen. It was also found that the minimum measured tensile force was in multiples of 3.9 nN. TEM images, force, and conductance measurements from the experiments are shown in Fig. 3.18. This kind of study indicates that the TEMAFM should be an ideal tool for studying atomic scale wires.

Such atomic sized TEMAFM experiments have also been performed for other studies such as on palladium [129] and iridium [130] atomic wide wires. Gold atomic wires have also been studied using a conductance feedback loop to maintain a constant number of electron transport channels [131]. Using basically the same setup, larger contacts for different materials have also been studied. For example, the correlation between stress and electromigration for copper [132, 133] and slip during tensile deformation of palladium [134] and silicon contacts [135, 136] have been investigated.

3.4.3.4 Friction and Adhesion

Friction between sliding bodies is the result of the formation, deformation, and breaking of a large number of contacts between two bodies. There has been a major

burst of activity in studies of friction since 1987, when the first standard AFM study of friction was done (for reviews, see [137–139]). With the standard AFM, single contacts are being studied, which may provide insight to the microscopic origin of friction. However, it is the real contact area that is, along with the loading force, of key importance in understanding friction, and, as noted earlier, the contact area information is only indirectly accessible using standard AFM instruments. Thus, the TEMAFM might give a unique opportunity to study friction using the TEM to image the contact area between the AFM tip and sample correlated with the friction and adhesion forces controlled by a loading force.

An early study of adhesion using TEMAFM [100] showed that the adhesive contact between two gold samples could best be described by the Maugis adhesion theory. Another observation in the same study was that the AFM jump-in-contact distance was larger than expected. The observed value of the jump-in-contact distance did not agree with the calculated value. The parameters to calculate the jump distance, the tip–sample distance, and the radius of tip and sample, are all observable by TEM, in contrast to standard AFM where the true tip–sample is unknown, and the tip radius can only be measured before and after the actual experiment using high-resolution microscopes. This larger distance was due to the migration of gold atoms into the gap by the attractive van der Waals forces. This work was done using a simple spring AFM cantilever, and the motion of the AFM tip, as viewed by TEM, gave a measure of the force. However, for extensive friction studies, a complete AFM setup is desired. Such a TEMAFM was used in the friction study by Fujusawa and Kizuka in 2003 [140], which focused on the frictional tip effect during AFM scanning and a small lateral displacement of the AFM tip during imaging. This displacement was shown to have an effect on the force–displacement plots and the scanned image when the scan size was in the same order as the lateral displacement.

3.5 Combined TEM and SPM Sample Preparation

One major difference between conventional TEM and TEMSPM samples is that for TEMSPM experiments both sample and SPM tip have to be placed orthogonally with respect to the electron beam for imaging, all the while keeping the electron transparent part of the TEM sample accessible to the SPM tip. Conventional TEM grids are therefore not practical to use for in situ TEM manipulation. For in situ TEM applications, a wire is normally used as support on which samples and custom-made substrates can be glued onto. Figure 3.19 shows sketches of common types of sample mountings used for in situ TEM manipulation. These sample preparation methods and STM probe preparation will be discussed in this section; however, AFM probes will not be addressed, as they are in most cases purchased and are generally not altered by the researchers themselves. More information on electrical AFM force sensors where a specialized MEMS fabrication scheme may be required can be found in Sect. 3.4.

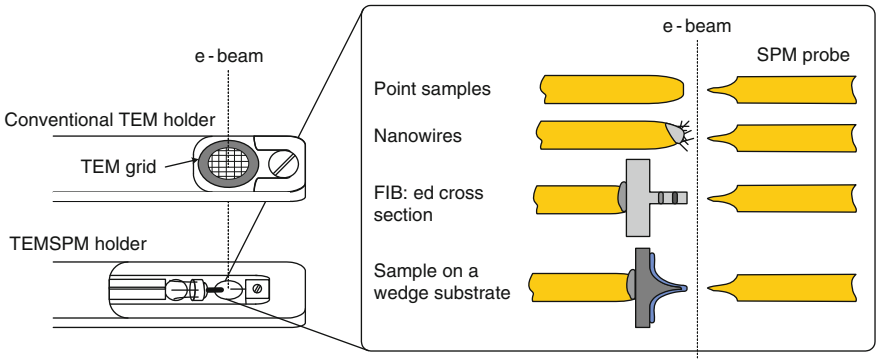

Fig. 3.19 Sketches of a conventional TEM holder, TEMSPM holder, and samples prepared for in situ TEM probing

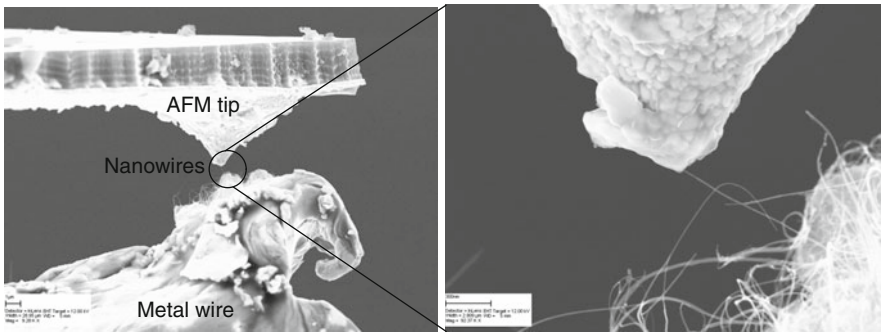

Fig. 3.20 Nanowires glued on a metallic wire ready for TEMSPM experiments

3.5.1 Nanowires and Nanoparticles

As shown throughout this chapter, nanowires are a common sample in TEMSPM experiments. Compared to conventional TEM samples, nanowires already possess the thin cross section required for electron transmission, and thus the sample can be prepared in a matter of minutes. The standard method is to use electrically conductive glue to ensure a reliable electrical and mechanical contact as in [60, 92]. The procedure is to dip the supporting wire, often an inert metal wire cut with a pair of scissors at an angle, into electrically conductive glue and then dip this conducting glue wire into a powder of nanowires or nanotubes [141]. An SEM image of nanowires attached to a support wire can be seen in Fig. 3.20.

Another simple way to prepare nanowire samples is to dip the supporting wire directly in the nanowire powder and simply let the surface adhesion forces keep the nanowires in place [142]. Hirayama et al. [82], for example, used an ethanol solution of single-walled carbon nanotubes to prepare a tip in this way. If a single nanowire is needed, in contrast to the large number of nanowires obtained by method described

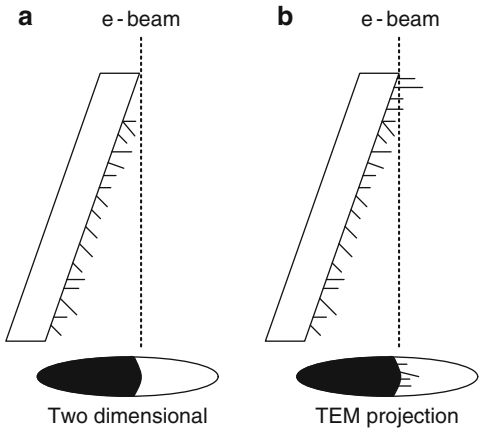

Fig. 3.21 Nanowire grown on a flat substrate. (**a**) Sketch of the TEM image when the nanowires shadow the projection image. (**b**) Sketch of the TEM image when the nanowires are not shadowed by the substrate

above, which might be desired if both contact regions are to be investigated, a more elaborate method is needed. A single nanowire can be of interest when both contact regions are to be investigated. In [143], a SEM-FIB equipped with a nanomanipulator was used to extract a single carbon nanotube, and the FIB was used to weld it to a gold wire.

There have also been reports on nanowires grown directly on a metallic wire as in [92, 144]. This type of sample is ideal for TEMSPM experiments. The wires already have a good mechanical and electrical contact to the wire and are easily accessible by an SPM probe.

For nanowires grown directly on a silicon substrate, the substrate needs to first be broken into smaller parts, typically 2 mm × 2 mm. Here it is important to note that because the substrate will always be mounted at a small angle; only nanowires on the edge of the substrate will be seen in the two-dimensional projection image obtained in the TEM, as illustrated in Fig. 3.21. Consequently, the substrate must be cut in a way that does not damage the nanowires at the edges. Standard diamond dicing is generally not a delicate enough method to use, as there is both cooling water present and chipping on the edges of the sample that can damage the nanowires. An alternative method is to cleave the substrate using a side cutter at the edge of the sample and let the silicon break along its path. Thus, the nanowires along the cleaved edge are not damaged. This sample preparation technique has been used in [50], among others.

To study nanoparticles with TEMSPM the sample can be prepared in several ways. There are examples when nanoparticles have been directly deposited on a wedge type substrate as seen in Fig. 3.27 [145] or they can be dispersed on a flat surface as done in [146]. One simple and common method to prepare the samples is to let a drop of solution of the nanoparticles dry on a TEM grid. This technique is also applicable in TEMSPM, but with the grid replaced by a tip or a half grid.

An alternative method to measure on nanoparticles is to grow them directly on nanowires or nanotubes. Zhang et al. [147] have made a simple, water based, protocol for growing gold nanoparticles on carbon nanotubes. A gold salt is reduced by

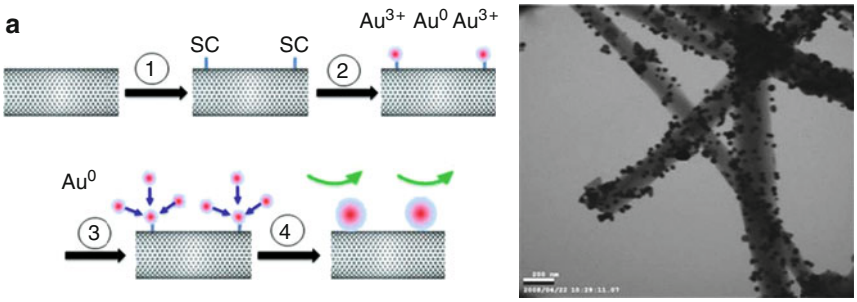

Fig. 3.22 Schematic drawing for synthesizing of gold nanoparticles on carbon nanotubes. (**a**) The procedure of preparing carbon nanotubes with gold particles is shown here. Carbon nanotubes were first premixed with sodium citrate (SC) by ultrasonication (1). $HAuCl_4$ was added into the reaction system causing reduction of Au^{3+} ions to Au^0 (2). The reduced gold atom on the carbon nanotube acts as a seed for self-assembling of other gold atoms (3). Gold nanoparticles are deposited on the carbon nanotube (4). (**b**) A TEM image of 30 nm gold nanoparticles decorating carbon nanotubes. Images are from [147]

sodium citrate and allowed to grow on carbon nanotubes, as seen in Fig. 3.22. The size and density of the nanoparticles could be altered by changing the concentrations of the solvents. The method is not restricted to carbon nanotubes but is generally applicable; for example, nanowires of $Mo_6S_3I_6$ [76] and clay particles [148] can be decorated by gold nanoparticles in this way. Other kinds of nanoparticles, such as platinum, palladium, or silver might be deposited in a similar way [149].

3.5.2 A Proper Electrical Contact for TEMSPM

The best way to make an electrode for electrical probing in a TEMSTM is to mechanically cut a wire from an inert metal such as gold or platinum. A common procedure is to use a pair of scissors or small wire cutters and cut the wire at a 45° angle. This will produce a rough tip with a large number of clean asperities on the nanoscale. Inside the TEM, one of these nanotips closest to the sample is used for probing.

Etched probes are usually more difficult to use and require elaborate cleaning steps. One reason to use an etched tip is that it provides a better geometry in cases where a high aspect ratio tip is required to reach the area of interest. Such etched wires can also be very sharp, with a tip radius as low as 5 nm [150]. In standard STM, the cut tips are the most common, but when operating the STM in UHV, electropolished tungsten is also a common tip. The electropolished tungsten tips are covered with a tungsten oxide layer, but in UHV this layer can be sublimated away at 800°C by heating it with a field emission current [151]. Gold can also be electropolished, but the procedure normally leaves a nanometer contamination layer

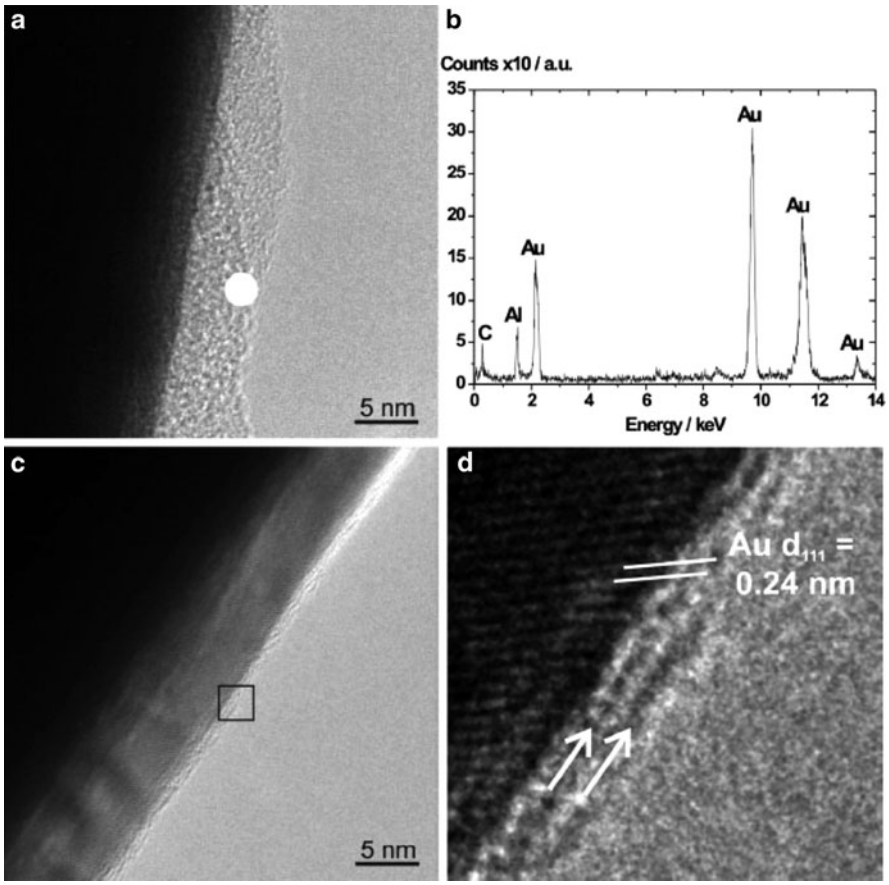

Fig. 3.23 (**a**) An electropolished gold tip with a contamination layer on the surface making it hard to make a proper electrical contact. (**b**) An EDS measurement showing that the contamination layer contains carbon. (**c**) A mechanically cut wire is shown to be more clean. (**d**) Here a carbon layer, 1 nm is seen on the cut gold electrode. Images are from [152]

thick as shown by Costa et al. [152]. Figure 3.23a shows this contamination layer, and the cleanliness of the simple cutting technique is demonstrated in Fig. 3.23c.

An indicator of bad electrical contact between two metals is a nonlinear I–V curve, whereas a proper contact will produce a linear curve, as seen in Fig. 3.24. Such nonlinearity is a signature of a tunneling barrier. The nonlinearity is due to the fact that the applied voltage will change the tunneling barrier. At higher bias voltage, the barrier will be both lower and thinner and thereby increase the tunneling probability and the electron current [153]. This tunneling barrier often originates from contaminations in the form of hydrocarbons present in the air and in the residual gases of the TEM column. This is seen in Fig. 3.23d, where a thin carbon layer is present on the mechanically cut gold wire. One way to remove such contaminations

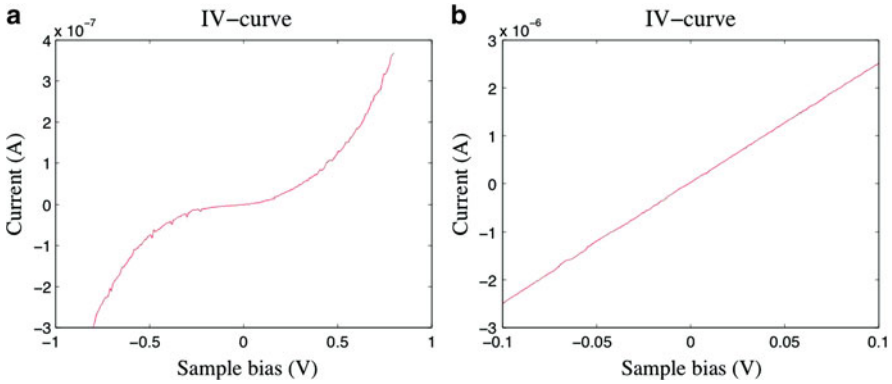

Fig. 3.24 (**a**) Typical nonlinear I–V curve for a bad contact. The curve is symmetric around zero voltage. (**b**) A proper contact. Image is from [143]

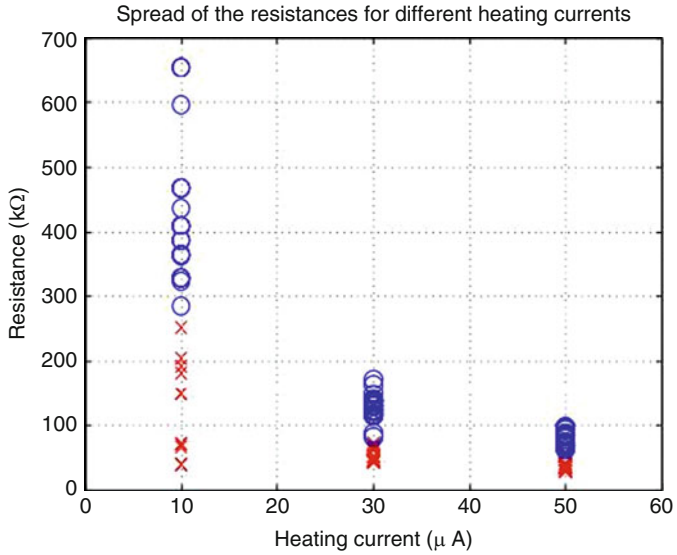

Fig. 3.25 Resistance vs. heating current, along different positions for two separate carbon nanotubes. Image is from [143]

in situ is to apply a high current which leads to Joule heating. This process is self-adjusting because the highest heating power will be dissipated where the highest resistance is present in the circuit ($P = RI^2$), that is, the location of the high ohmic tunneling barrier. Such an effect is shown in Fig. 3.25 where the high-ohmic contact between a carbon nanotube and a gold tip is lowered by increasing the current.

One further consideration regarding electrical contacts in the TEM is the effect of the electron beam on the hydrocarbon contamination layer inside the TEM chamber.

It is well known that when the contamination layer inside the electron microscope is exposed to the electron beam, a growth of a-C will occur there. This phenomenon, EBID, could be used for growing structures but could also result in a bad electrical contact. When the TEM electron beam irradiates a surface, the hydrocarbon will decompose leaving a stable a-C layer behind. More hydrocarbons will quickly cover the a-C structure and if the area is exposed further, the a-C structure will grow in thickness. As shown by Peng et al. [154], the hydrocarbon contamination layer could be evaporated away by Joule heating and thus inhibit the EBID effect. At a temperature of 430°C the EBID process disappeared, pointing at a way to keep a sample clean under high vacuum conditions.

3.5.3 Lamella Samples

For the study of bulk materials or heterogenic sandwich structures with TEMSPM techniques, the sample needs to be in the shape of a thin lamella. For TEMSPM, while it is important that the lamella is thin enough for TEM imaging, it should also be well supported so that it does not bend when a force is applied. If the rear parts of the sample bend, this could change the characteristics of the sample in unintended areas. For example, in a TEMSTM study of magnetic tunnel junctions [155], H-bar shaped electron transparent windows were prepared using FIB. These electron transparent windows were 15 μm across and measured 100 nm in thickness. By using windows, the structure becomes more stable and easily accessible with an STM tip. In another work, a cross section of a $LaAlO_3/SrTiO_3$ thin heterostructure film was measured using TEMSTM [156]. The sample preparation, TEM images, and I–V curves are seen in Fig. 3.26. This sample was prepared by grinding and ion milling. The FIB was not used in this case because the implanted ions from the ion beam could alter the electrical properties. As seen in Fig. 3.26a, the geometry of the sample was prepared such that the STM tip could contact the electron transparent region while being imaged in the same plane.

An alternative way of investigating thin films is to directly deposit a film on a micromachined substrate [18, 157]. An example of such a substrate is seen in Fig. 3.27. By using micromachining, the substrate can be designed to have a steady support and an electron transparent edge. The investigated material can then be deposited directly on the substrate and, if needed, further modified using FIB.

3.5.4 Electron Beam Irradiation Effects

Another issue regarding in situ TEM measurement is the impact of using a high energy electron beam on the sample. The energy of an electron beam used in the TEM is typically 100–300 keV, and this can damage the samples during image

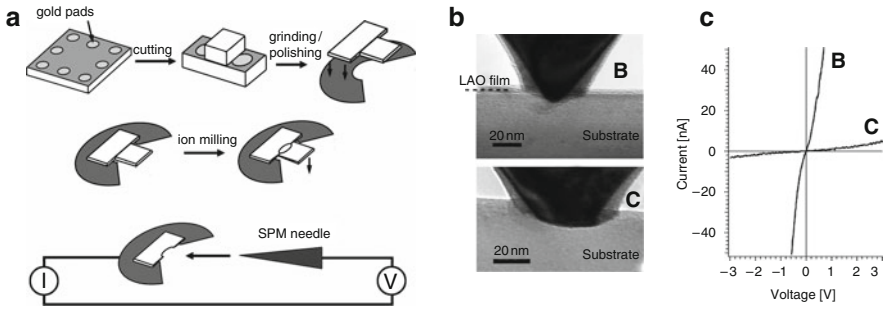

Fig. 3.26 (**a**) The procedure of how a $LaAlO_3/SrTiO_3$ thin film was prepared for TEMSTM measurements. First, a cross section of a macro sample is cut, and then it is thinned down and attached to a support shaped as a half TEM grid. The sample is further thinned to expose an electron transparent area. (**b**) TEM images of the prepared sample and I–V curve taken. Images are from [156]

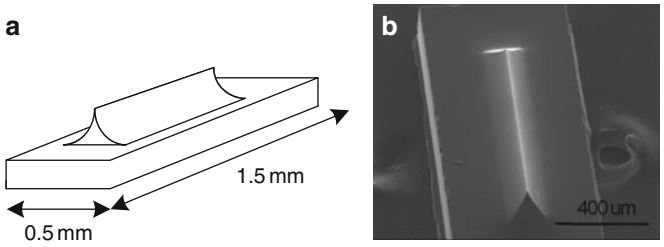

Fig. 3.27 A silicon substrate for TEM sample mounting. (**a**) A sketch of a wedge shaped silicon structure. (**b**) A SEM image of the silicon wedge. Images are from [157]

acquisition. The magnitude of this ever present effect depends on the kinetic energy of the electrons, the current density at the sample, and the accumulated dose [158]. This phenomenon might be useful as in the work of Takayanagi et al. [39] where they thinned down a gold film until only single atom wide wires remained, or as in the studies by Jin et al. [159] where graphene was modified until a single wire of carbon remained. Another example, by Ugarte, is the creation of carbon onions by irradiating a-C [160]. While a high energy electron beam can be useful, it is also more important to be aware of the electron irradiation in order to not alter the specimen under study (for a review, see [161]). For example, carbon nanotubes imaged at 200 kV in a TEM will quickly be destroyed as shown in [161]. One solution is to decrease the acceleration voltage in the TEM; for the case of carbon nanotubes a voltage below 120 kV is recommended as this is the threshold for knock on damage. However, even below that threshold there are still effects from the electron beam, as can be seen in Fig. 3.28. The carbon nanotube in Fig. 3.28 was intentionally exposed a prolonged period to 80 keV.

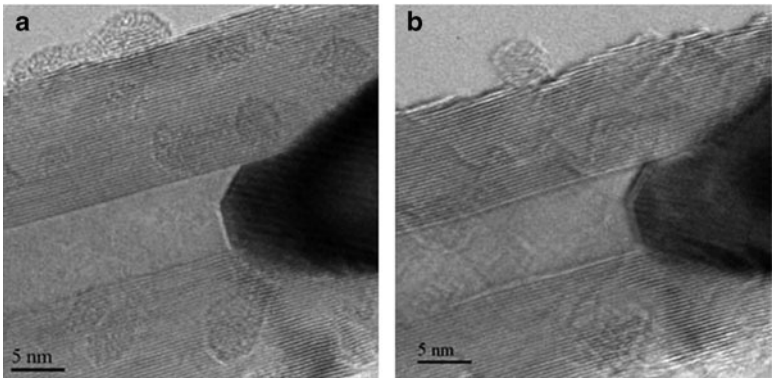

Fig. 3.28 TEM images of iron filled multiwall carbon nanotubes. (**a**) Before prolonged exposure to the electron beam. (**b**) After prolonged electron beam irradiation at 80 keV impact energy

3.6 Conclusion

With the addition of TEM capabilities to the already established STM and AFM techniques, many new possibilities have emerged. As the SPM analysis and manipulation of the sample now can be followed in real time by high resolution imaging in TEM, experimental data that was not previously accessible can be extracted.

In the case of TEMSTM, the use of TEM has increased the fundamental understanding of the tip–sample interaction and has been instrumental in the analysis of materials on the nanoscale. For example, single atom chains have been created and analyzed, electrical properties of single nanoscale structures have been investigated, and details of electromigration phenomena have been revealed. In many cases, the combination of TEM and STM has enabled the use of the STM in completely new ways, such as using the tip for Joule heating of nanowires or welding of carbon nanotubes.

By combining TEM and AFM to TEMAFM, a nanoforce detection system capable of investigating the mechanical properties of individual nanostructures has been created. When correlating the real-time monitoring in the TEM with the force–displacement data from the AFM, details about the deformation mechanisms can be obtained, explaining features in the mechanical data. The analysis of mechanical properties of single nanotubes and nanowires, studies of nanoscale friction, and fracture was for the first time enabled by the TEMAFM.

With TEMSPM techniques, now more than ever before, more detailed data about nanostructures are accessible and the development of such techniques and their applications hold great promises for development of new materials with significantly different properties than previously possible.

References

1. M. Iwatsuki, K. Murooka, S. Kitamura, K. Takayanagi, Y. Harada, Scanning tunneling microscope (STM) for conventional transmission electron microscope (TEM). J. Electron Microsc. **40**, 48–53 (1991)
2. Y. Naitoh, K. Takayanagi, M. Tomitori, Visualization of tip-surface geometry at atomic distance by TEM-STM holder. Surf. Sci. **357–358**, 208–212 (1996)
3. D. Erts, A. Lohmus, R. Lohmus, H. Olin, Instrumentation of STM and AFM combined with transmission electron microscope. Appl. Phys. A Mater. Sci. Process. **72**, S71–S74 (2001)
4. K. Takayanagi, Y. Kondo, H. Ohnishi, Suspended gold nanowires: ballistic transport of electrons. JSAP Int. **3**, 3–8 (2001)
5. M. Sveningsson, K. Hansen, K. Svensson, E. Olsson, E. Campbell, Quantifying temperature-enhanced electron field emission from individual carbon nanotubes. Phys. Rev. B. **72** (2005)
6. Z.L. Wang, P. Poncharal, W.A. de Heer, Nanomeasurements in transmission electron microscopy. Microsc. Microanal. **6**, 224–230 (2000)
7. Z.L. Wang, P. Poncharal, W.A. de Heer, Measuring physical and mechanical properties of individual carbon nanotubes by in situ TEM. J. Phys. Chem. Solids. **61**, 1025–1030 (2000)
8. Z.L. Wang, R.P. Gao, Z.W. Pan, Z.R. Dai, Nano-scale mechanics of nanotubes, nanowires, and nanobelts. Adv. Eng. Mater. **3**, 657 (2001)
9. X. Han, Z. Zang, Z.L. Wang, Experimental nanomechanics of onedimensional nanomaterials by in situ microscopy. Nano: Briefs Rev. **2**, 249–271 (2007)
10. D. Golberg, P.M. Costa, M. Mitome, Y. Bando, Properties and engineering of individual inorganic nanotubes in a transmission electron microscope. J. Mater. Chem. **19**, 909 (2009)
11. L. Dong, A. Subramanian, B.J. Nelson, Carbon nanotubes for nanorobotics. Nano Today. **2**, 12–21 (2007)
12. L. Dong, K. Shou, D.R. Frutiger, A. Subramanian, L. Zhang, B.J. Nelson, X. Tao, X. Zhang, Engineering multiwalled carbon nanotubes inside a transmission electron microscope using nanorobotic manipulation. IEEE Trans. Nanotechnol. **7**, 508–517 (2008)
13. L. Dong, X. Tao, L. Zhang, X. Zhang, B.J. Nelson, Plumbing the depths of the nanometer scale. IEEE Nanotechnol. Mag. **4**, 13–22 (2010)
14. "MRS BULLENTIN," MRS Bull. **33** (2008)
15. M. Kociak, M. Kobylko, S. Mazzucco, R. Bernard, A.Y. Kasumov, C. Colliex, TEM nanolaboratory. Imaging Microsc. **10**, 26–27 (2008)
16. F. Banhart, *In-Situ Electron Microscopy at High Resolution* (World Scientific, Singapore, 2008)
17. E.A. Stach, In-situ TEM – a tool for quantitative observations of deformation behavior in thin films and nano-structured materials. Workshop on new materials science enabled by in situ microscopies, DOE BES, 2001
18. E.A. Stach, T. Freeman, A. Minor, D.K. Owen, J. Cumings, M. Wall, T. Chraska, R. Hull, J. Morris, A. Zettl, U. Dahmen, Development of a nanoindenter for in situ transmission electron microscopy. Microsc. Microanal. **7**, 507–517 (2001)
19. A.M. Minor, S.A. Asif, Z. Shan, E.A. Stach, E. Cyrankowski, T.J. Wyrobek, O.L. Warren, A new view of the onset of plasticity during the nanoindentation of aluminium. Nat. Mater. **5**, 697–702 (2006)
20. R. Gupta, R.E. Stallcup, in *Introduction to In Situ Nanomanipulation for Nanomaterials Engineering*, ed. by W. Zhou, Z.L. Wang. Scanning Microscopy for Nanotechnology – Techniques and Applications (Springer, Heidelberg, 2007), pp. 192–223
21. T. Kizuka, H. Ohmi, T. Sumi, K. Kumazawa, S. Deguchi, M. Naruse, S. Fujusawa, A. Yabe, Y. Enomoto, Simultaneous observation of millisecond dynamics in atomistic structure, force and conductance on the basis of transmission electron microscopy. Jpn. J. Appl. Phys. **40**, 170–173 (2001)
22. R. Young, The topografiner: an instrument for measuring surface microtopography. Rev. Sci. Instrum. **43**, 999 (1972)

23. G. Binnig, H. Rohrer, Surface imaging by scanning tunneling microscopy. Ultramicroscopy. **11**, 157–160 (1983)
24. C.J. Chen, *Introduction to Scanning Tunneling Microscopy* (Oxford University Press, Oxford, 1993)
25. C. Gerber, G. Binnig, H. Fuchs, O. Marti, H. Rohrer, Scanning tunneling microscope combined with a scanning electron microscope. Rev. Sci. Instrum. **57**, 221–224 (1986)
26. T. Ichinokawa, Y. Miyazaki, Y. Koga, Scanning tunneling microscope combined with scanning electron microscope. Ultramicroscopy. **23**, 115–118 (1987)
27. J.C. Spence, A scanning tunneling microscope in a side-entry holder for reflection electron microscopy in the Philips EM400. Ultramicroscopy. **25**, 165–169 (1988)
28. W.K. Lo, J.C. Spence, Investigation of STM image artifacts by in situ reflection electron microscopy. Ultramicroscopy, **48**, 433–444 (1993)
29. H. Ohnishi, Y. Kondo, K. Takayanagi, UHV electron microscope and simultaneous STM observation of gold stepped surfaces. Surf. Sci. **415**, L1061–L1064 (1998)
30. Y. Oshima, K. Mouri, H. Hirayama, K. Takayanagi, Development of a miniature STM holder for study of electronic conductance of metal nanowires in UHV–TEM. Surf. Sci. **531**, 209–216 (2003)
31. Z.L. Wang, P. Poncharal, W.A. de Heer, Nanomeasurements of individual carbon nanotubes by in situ TEM. Pure Appl. Chem. **72**, 209–219 (2000)
32. R. Lohmus, D. Erts, A. Lohmus, K. Svensson, Y. Jompol, H. Olin, STM and AFM instrumentation combined with transmission electron microscope. Phys. Low-Dimensional Struct. **3–4**, 81–89 (2001)
33. M.I. Lutwyche, Y. Wada, Manufacture of micromechanical scanning tunneling microscopes for observation of the tip avex in a transmission electron microscope. Sens. Actuat. A: Phys. **48**, 127–136 (1995)
34. Y. Xu, N.C. Macdonald, S.A. Miller, Integrated micro-scanning tunneling microscope. Appl. Phys. Lett. **67**, 2305 (1995)
35. K. Svensson, Y. Jompol, H. Olin, E. Olsson, Compact design of a transmission electron microscope-scanning tunneling microscope holder with three-dimensional coarse motion. Rev. Sci. Instrum. **74**, 4945 (2003)
36. "Nanofactory Instruments; www.nanofactory.com."
37. J.C. Spence, W. Lo, M. Kuwabara, Observation of the graphite surface by reflection electron microscopy during STM operation. Ultramicroscopy, **33**, 69–82 (1990)
38. W. Lo, J.C. Spence, Investigation of STM image artifacts by in-situ reflection electron microscopy. Ultramicroscopy, **48**, 433–444 (1993)
39. H. Ohnishi, Y. Kondo, K. Takayanagi, Quantized conductance through individual rows of suspended gold atoms. Nature. **395**, 2–5 (1998)
40. N. Agraït, A.L. Yeyati, J.M. van Ruitenbeek, Quantum properties of atomic-sized conductors. Phys. Rep. **377**, 81–279 (2003)
41. Y. Kurui, Y. Oshima, M. Okamoto, K. Takayanagi, Integer conductance quantization of gold atomic sheets. Phys. Rev. B. **77** (2008)
42. Y. Kurui, Y. Oshima, M. Okamaoto, K. Takayanagi, Conductance quantization/dequantization in gold nanowires due to multiple reflection at the interface. Phys. Rev. B. **79**, 165414 (2009)
43. K. Takayanagi, Y. Oshima, Y. Kurui, Conductance quantization of gold nanowires as a ballistic conductor. Phys. Rev. Lett. **2**, 47–50 (2009)
44. D. Erts, H. Olin, L. Ryen, E. Olsson, A. Thölén, Maxwell and Sharvin conductance in gold point contacts investigated using TEM-STM. Phys. Rev. B, **61**, 12725–12727 (2000)
45. Z. Aslam, M. Abraham, R. Brydson, A. Brown, B. Rand, Initial studies using a combined TEM – scanning tunnelling microscopy (STM) side entry sample holder. J. Phys.: Conf. Ser. **26**, 54–58 (2006)
46. Z. Aslam, M. Abraham, A. Brown, B. Rand, R. Brydson, Electronic property investigations of single-walled carbon nanotube bundles in situ within a transmission electron microscope: an evaluation. J. Microsc. **231**, 144–155 (2008)
47. J. Cumings, A. Zettl, Field emission and current-voltage properties of boron nitride nanotubes. Solid State Commun. **129**, 661–664 (2004)

48. S. Frank, P. Poncharal, Z.L. Wang, W.A. de Heer, Carbon nanotube quantum resistors. Science. **280**, 1744–1746 (1998)
49. H.U. Strand, K. Svensson, E. Olsson, Critical aspects of liquid metal immersion methods for characterization of electron transport properties in carbon nanotubes. In preparation
50. M.W. Larsson, L.R. Wallenberg, A.I. Persson, L. Samuelson, Probing of individual semiconductor nanowhiskers by TEM-STM. Microsc. Microanal. **10**, 41–46 (2004)
51. T. Kuzumaki, H. Yasuhiro, T. Kizuka, In-situ atomistic observation of carbon nanotubes during field emission. AIP Conf. Proc. 281–284 (2001)
52. T. Kuzumaki, H. Sawada, H. Ichinose, Y. Horiike, T. Kizuka, Selective processing of individual carbon nanotubes using dual-nanomanipulator installed in transmission electron microscope. Appl. Phys. Lett. **79**, 4580–4582 (2001)
53. T. Kuzumaki, Y. Horiike, T. Kizuka, T. Kona, C. Oshima, Y. Mitsuda, The dynamic observation of the field emission site of electrons on a carbon nanotube tip. Diamond Relat. Mater. **13**, 1907–1913 (2004)
54. J. Cumings, A. Zettl, M.R. McCartney, J.C. Spence, Electron holography of field-emitting carbon nanotubes. Phys. Rev. Lett. **88**, 1–4 (2002)
55. M. Wang, Q. Chen, L. Peng, Grinding a nanotube. Adv. Mater. **20**, 724–728 (2008)
56. R.P. Gao, Z.W. Pan, Z.L. Wang, Work function at the tips of multiwalled carbon nanotubes. Appl. Phys. Lett. **78**, 1757–1759 (2001)
57. X. Bai, E.G. Wang, P. Gao, Z.L. Wang, Measuring the work function at a nanobelt tip and at a nanoparticle surface. Nano Lett. **3**, 1147–1150 (2003)
58. Z. Xu, X.D. Bai, E.G. Wang, Z.L. Wang, Field emission of individual carbon nanotube with in situ tip image and real work function. Appl. Phys. Lett. **87**, 163106 (2005)
59. Z. Xu, X.D. Bai, E.G. Wang, Z.L. Wang, Dynamic in situ field emission of a nanotube at electromechanical resonance. J. Phys.: Condens. Matter. **17**, L507–L512 (2005)
60. K. Svensson, H. Olin, E. Olsson, Nanopipettes for metal transport. Phys. Rev. Lett. **93**, 14590 (2004)
61. B.C. Regan, S. Aloni, R.O. Ritchie, U. Dahmen, A. Zettl, Carbon nanotubes as nanoscale mass conveyors. Nature. **428**, 924–927 (2004)
62. L. Dong, X. Tao, L. Zhang, X. Zhang, B.J. Nelson, Nanorobotic spot welding: controlled metal deposition with attogram precision from copper-filled carbon nanotubes. Nano Lett. **7**, 58–63 (2007)
63. L. Dong, X. Tao, M. Hamdi, L. Zhang, X. Zhang, A. Ferreira, B.J. Nelson, Nanotube fluidic junctions: internanotube attogram mass transport through walls. Nano Lett. **9**, 210–214 (2009)
64. P.M. Costa, D. Golberg, M. Mitome, S. Hampel, A. Leonhardt, B. Buchner, Y. Bando, Stepwise current-driven release of attogram quantities of copper iodide encapsulated in carbon nanotubes. Nano Lett. **8**, 3120–3125 (2008)
65. G.E. Begtrup, W. Gannett, T.D. Yuzvinsky, V.H. Crespi, A. Zettl, Nanoscale reversible mass transport for archival memory. Nano Lett. **9**, 1835–1838 (2009)
66. J.Y. Huang, S. Chen, Z.F. Ren, G. Chen, M.S. Dresselhaus, Real-time observation of tubule formation from amorphous carbon nanowires under high-bias Joule heating. Nano Lett. **6**, 1699–1705 (2006)
67. S. Chen, J.Y. Huang, Z. Wang, K. Kempa, G. Chen, Z.F. Ren, High-bias-induced structure and the corresponding electronic property changes in carbon nanotubes. Appl. Phys. Lett. **87**, 263107 (2005)
68. J. Huang, S. Chen, Z.Q. Wang, K. Kempa, Y.M. Wang, S.H. Jo, G. Chen, M.S. Dresselhaus, Z.F. Ren, Superplastic carbon nanotubes. Nature. **439**, 281 (2006)
69. J.Y. Huang, S. Chen, S.H. Jo, Z. Wang, D.X. Han, G. Chen, M.S. Dresselhaus, Z.F. Ren, Atomic-scale imaging of wall-by-wall breakdown and concurrent transport measurements in multiwall carbon nanotubes. Phys. Rev. Lett. **94**, 236802 (2005)
70. T.D. Yuzvinsky, W. Mickelson, S. Aloni, G.E. Begtrup, A. Kis, A. Zettl, Shrinking a carbon nanotube. Nano Lett. **6**, 2718–2722 (2006)
71. J.Y. Huang, F. Ding, B.I. Yakobson, P. Lu, L. Qi, J. Li, In situ observation of graphene sublimation and multi-layer edge reconstructions. Proc. Natl Acad. Sci. USA. **106**, 10103–10108 (2009)

72. K. Saito, J. Fujii, T. Kizuka, Electric conduction of amorphous carbon and graphitic nanocontacts. Jpn. J. Appl. Phys. **48**, 010218 (2009)
73. T. Westover, R. Jones, J.Y. Huang, G. Wang, E. Lai, A. Talin, Photoluminescence, thermal transport, and breakdown in joule-heated GaN nanowires. Nano Lett. **9**, 257–263 (2009)
74. Z. Xu, D. Golberg, Y. Bando, Electrical field-assisted thermal decomposition of boron nitride nanotube: experiments and first principle calculations. Chem. Phys. Lett. **480**, 110–112 (2009)
75. Z. Xu, D. Golberg, Y. Bando, In situ TEM-STM recorded kinetics of boron nitride nanotube failure under current flow. Nano Lett. **9**, 2251–2254 (2009)
76. M. Hummelgård, R. Zhang, T. Carlberg, D. Vengust, D. Dvorsek, D. Mihailovic, H. Olin, Nanowire transformation and annealing by Joule heating. Nanotechnology. **21**, 165704 (2010)
77. J. Yamashita, H. Hirayama, Y. Ohshima, K. Takayanagi, Growth of a single-wall carbon nanotube in the gap of scanning tunneling microscope. Appl. Phys. Lett. **74**, 2450–2452 (1999)
78. M. Yoshida, Y. Kurui, Y. Oshima, K. Takayanagi, In-Situ observation of the fabrication process of a single shell carbon fullerene nano-contact using transmission electron microscope–scanning tunneling microscope. Jpn. J. Appl. Phys. **46**, L67–L69 (2007)
79. R. Zhang, M. Hummelgård, H. Olin, Carbon nanocages grown by gold templating. Carbon **48**, 424–430 (2010)
80. T. Kizuka, R. Kato, K. Miyazawa, Structure of hollow carbon nanocapsules synthesized by resistive heating. Carbon **47**, 138–144 (2009)
81. C.H. Jin, J.Y. Wang, Q. Chen, L.M. Peng, In situ fabrication and graphitization of amorphous carbon nanowires and their electrical properties. J. Phys. Chem. B. **110**, 5423–5428 (2006)
82. H. Hirayama, Y. Kawamoto, Y. Ohshima, K. Takayanagi, Nanospot welding of carbon nanotubes. Appl. Phys. Lett. **79**, 1169 (2001)
83. C. Jin, K. Suenaga, S. Iijima, Plumbing carbon nanotubes. Nat. Nanotechnol. **3**, 17–21 (2008)
84. M. Wang, L. Peng, J. Wang, Q. Chen, Shaping carbon nanotubes and the effects on their electrical and mechanical properties. Adv. Funct. Mater. **16**, 1462–1468 (2006)
85. D.N. Madsen, K. Mølhave, R. Mateiu, A.M. Rasmussen, M. Brorson, C.J. Jacobsen, P. Bøggild, Soldering of nanotubes onto microelectrodes. Nano Lett. **3**, 47–49 (2003)
86. L. de Knoop, K. Svensson, H. Petterson, E. Olsson, Extraction and local probing of individual carbon nanotubes. AIP Conference Proceedings, Aip, 2005, pp. 118–123
87. P. Poncharal, Electrostatic deflections and electromechanical resonances of carbon nanotubes. Science. **283**, 1513–1516 (1999)
88. R.P. Gao, Z.L. Wang, Z. Bai, W.A. de Heer, L. Dai, M. Gao, Nanomechanics of individual carbon nanotubes from pyrolytically grown arrays. Phys. Rev. Lett. **85**, 622–625 (2000)
89. M.M. Treacy, T.W. Ebbesen, J.M. Gibson, Exceptionally high Young's modulus observed for individual carbon nanotubes. Nature. **381**, 678–680 (1996)
90. J. Cumings, A. Zettl, Low-friction nanoscale linear bearing realized from multiwall carbon nanotubes. Science. **289**, 602–604 (2000)
91. T. Kizuka, Atomistic visualization of deformation in gold. Phys. Rev. B. **57**, 11158–11163 (1998)
92. K.J. Ziegler, D. Lyons, J.D. Holmes, D. Erts, B. Polyakov, H. Olin, K. Svensson, E. Olsson, Bistable nanoelectromechanical devices. Appl. Phys. Lett. **84**, 4074 (2004)
93. J. Andzane, N. Petkov, A.I. Livshits, J.J. Boland, J.D. Holmes, D. Erts, Two-terminal nanoelectromechanical devices based on germanium nanowires. Nano Lett. **9**, 1824–1829 (2009)
94. J. Andzane, J. Prikulis, D. Dvorsek, D. Mihailovic, D. Erts, Two-terminal nanoelectromechanical bistable switches based on molybdenum-sulfur-iodine molecular wire bundles. Nanotechnology. **21**, 125706 (2010)
95. G. Binnig, C.F. Quate, C. Gerber, Atomic force microscope. Phys. Rev. Lett. **56**, 930 (1986)
96. A.V. Ermakop, E.L. Garfunkel, A novel AFM/STM/SEM. Rev. Sci. Instrum. **65**, 2653–2654 (1994)
97. U. Stahl, C.W. Yuan, A.L. de Lozanne, M. Tortonese, Atomic force microscope using piezoresistive cantilevers and combined with a scanning electron microscope. Appl. Phys. Lett. **65**, 2878 (1994)
98. K. Jensen, W. Mickelson, A. Kis, A. Zettl, Buckling and kinking force measurements on individual multiwalled carbon nanotubes. Phys. Rev. B. **76**, 1–5 (2007)

99. Y. Lu, J.Y. Huang, C. Wang, S. Sun, J. Lou, Cold welding of ultrathin gold nanowires. Nat. Nanotechnol. 1–7 (2010)
100. D. Erts, A. Lohmus, R. Lohmus, H. Olin, A.V. Pokropivny, L. Ryen, K. Svensson, Force interactions and adhesion of gold contacts using a combined atomic force microscope and transmission electron microscope. Appl. Surf. Sci. **188**, 460–466 (2002)
101. C.M. Mate, G.M. McClelland, R. Erlandsson, S. Chiang, Atomic-scale friction of a tungsten tip on a graphite surface. Phys. Rev. Lett. **59**, 1942 (1987)
102. Y. Martin, C.C. Williams, H.K. Wickramasinghe, Atomic force microscope-force mapping and profiling on a sub 100-Å scale. J. Appl. Phys. **61**, 4723 (1987)
103. G. Neubauer, S.R. Cohen, G.M. McClelland, D. Horne, C.M. Mate, Force microscopy with a bidirectional capacitance sensor. Rev. Sci. Instrum. **61**, 2296 (1990)
104. T. Go¨ddenhenrich, H. Lemke, U. Hartmann, C. Heiden, Force microscope with capacitive displacement detection. J. Vac. Sci. Technol. A: Vac. **8**, 383 (1990)
105. T. Itoh, T. Suga, Piezoelectric force sensor for scanning force microscopy. Engineering. **43**, 305–310 (1994)
106. M. Tortonese, R.C. Barrett, C.F. Quate, Atomic resolution with an atomic force microscope using piezoresistive detection. Appl. Phys. Lett. **62**, 834 (1993)
107. A. Nafari, A. Danilov, H. Rödjegård, P. Enoksson, H. Olin, A micromachined nanoindentation force sensor. Sens. Actuat. A: Phys. **123–124**, 44–49 (2005)
108. H.D. Espinosa, Y. Zhu, B. Peng, A MEMS device for in situ TEM/AFM/SEM/STM testing of carbon nanotubes and nanowires. 2002 SEM annual conference, Milwaukee, 2002, pp. 1–5
109. S.A. Asif, K.J. Wahl, R.J. Colton, Nanoindentation and contact stiffness measurement using force modulation with a capacitive load-displacement transducer. Rev. Sci. Instrum. **70**, 2408 (1999)
110. A. Nafari, D. Karlen, C. Rusu, K. Svensson, H. Olin, P. Enoksson, MEMS sensor for in situ TEM atomic force microscopy. J. Microelectromech. Syst. **17**, 328–333 (2008)
111. J. Thaysen, A. Boisen, O. Hansen, S. Bouwstra, Atomic force microscopy probe with piezoresistive read-out and a highly symmetrical Wheatstone bridge arrangement. Sens. Actuat. A: Phys. **83**, 47–53 (2000)
112. D. Golberg, P.M. Costa, O. Lourie, M. Mitome, X. Bai, K. Kurashima, C. Zhi, C. Tang, Y. Bando, Direct force measurements and kinking under elastic deformation of individual multiwalled boron nitride nanotubes. Nano Lett. **7**, 2146–2151 (2007)
113. A. Asthana, K. Momeni, A. Prasad, Y.K. Yap, R.S. Yassar, In situ probing of electromechanical properties of an individual ZnO nanobelt. Appl. Phys. Lett. **95**, 172106 (2009)
114. P.M. Costa, D. Golberg, G. Shen, M. Mitome, Y. Bando, ZnO low-dimensional structures: electrical properties measured inside a transmission electron microscope. J. Mater. Sci. **43**, 1460–1470 (2007)
115. T. Shokuhfar, G.K. Arumugam, P.A. Heiden, R.S. Yassar, C. Friedrich, Direct compressive measurements of individual titanium dioxide nanotubes. ACS Nano. **3**, 3098–3102 (2009)
116. T. Kuzumaki, Y. Mitsuda, Nanoscale mechanics of carbon nanotube evaluated by nanoprobe manipulation in transmission electron microscope. Jpn. J. Appl. Phys. **45**, 364–368 (2006)
117. X. Bai, D. Golberg, Y. Bando, C. Zhi, C. Tang, M. Mitome, K. Kurashima, Deformation-driven electrical transport of individual boron nitride nanotubes. Nano Lett. **7**, 632–637 (2007)
118. T. Kizuka, Direct atomistic observation of deformation in multiwalled carbon nanotubes. Phys. Rev. B. **59**, 4646–4649 (1999)
119. K. Asaka, R. Kato, K. Miyazawa, T. Kizuka, Deformation of multiwalled nanometer-sized carbon capsules. Appl. Phys. Lett. **89**, 191914 (2006)
120. H. Ghassemi, Y.K. Yap, R.S. Yassar, In-situ nanomechanical testing of one dimensional material. NSTI-Nanotech 2009, Houston (2009).
121. K. Asaka, K. Miyazawa, T. Kizuka, The toughness of multi-wall carbon nanocapsules. Nanotechnology. **20**, 385705 (2009)
122. R. Kato, K. Asaka, K. Miyazawa, T. Kizuka, In situ high-resolution transmission electron microscopy of elastic deformation and fracture of nanometer-sized fullerene C 60 whiskers. Jpn. J. Appl. Phys. **45**, 8024–8026 (2006)

123. K. Saito, K. Miyazawa, T. Kizuka, Bending process and Young's modulus of fullerene C 60 nanowhiskers. Jpn. J. Appl. Phys. **48**, 010217 (2009)
124. M.S. Wang, Y. Bando, J.A. Rodriguez-Manzo, F. Banhart, D. Golberg, Cobalt nanoparticle-assisted engineering of multiwall carbon nanotubes. ACS Nano. **3**, 2632–2638 (2009)
125. P.M. Costa, U.K. Gautam, M.S. Wang, Y. Bando, D. Golberg, Effect of crystalline filling on the mechanical response of carbon nanotubes. Carbon. **47**, 541–544 (2009)
126. S. Blom, H. Olin, J. Costa-Kramer, N. Garcia, M. Jonson, P. Serena, R. Shekhter, Free-electron model for mesoscopic force fluctuations in nanowires. Phys. Rev. B. **57**, 8830–8833 (1998)
127. N. Agraït, G. Rubio, S. Vieira, Plastic deformation of nanometer-scale gold connective necks. Phys. Rev. Lett. **74**, 3995–3998 (1995)
128. T. Kizuka, Atomic configuration and mechanical and electrical properties of stable gold wires of single-atom width. Phys. Rev. B. **77** (2008)
129. T. Matsuda, T. Kizuka, Palladium wires of single atom width as mechanically controlled switching devices. Jpn. J. Appl. Phys. **45**, L1337–L1339 (2006)
130. M. Ryu, T. Kizuka, Structure, conductance and strength of iridium wires of single atom width. Jpn. J. Appl. Phys. **45**, 8952–8956 (2006)
131. T. Matsuda, T. Kizuka, Structure and tensile force of nanometer- and atomic-sized gold contacts during conductance feedback control. Jpn. J. Appl. Phys. **48**, 125007 (2009)
132. S. Fujisawa, T. Kikkawa, T. Kizuka, Direct observation of electromigration and induced stress in Cu nanowire. Jpn. J. Appl. Phys. **42**, L1433–L1435 (2003)
133. T. Kizuka, H. Aoki, The dynamics of electromigration in copper nanocontacts. Appl. Phys. Express. **2**, 075003 (2009)
134. T. Matsuda, T. Kizuka, Slip sequences during tensile deformation of palladium nanocontacts. Jpn. J. Appl. Phys. **48**, 115003 (2009)
135. T. Kizuka, Y. Takatani, K. Asaka, R. Yoshizaki, Measurements of the atomistic mechanics of single crystalline silicon wires of nanometer width. Phys. Rev. B. **72**, 1–6 (2005)
136. T. Kizuka, Y. Takatani, Growth of silicon nanowires by nanometer-sized tip manipulation. Jpn. J. Appl. Phys. **46**, 5706–5710 (2007)
137. B.N. Persson, Sliding friction. Surf. Sci. Rep. **33**, 83–119 (1999)
138. E. Gnecco, R. Bennewitz, T. Gyalog, E. Meyer, Friction experiments on the nanometre scale. J. Phys.: Condens. Matter. **13**, R619–R642 (2001)
139. B. Bhushan, *Nanotribology and Nanomechanics* (Springer, Heidelberg, 2008)
140. S. Fujisawa, T. Kizuka, Lateral displacement of an AFM tip observed by in-situ TEM/AFM combined microscopy: the effect of the friction in AFM. Tribol. Lett. **15**, 163–168 (2003)
141. "Preparation of sample for in-situ tem-spm operation; www.youtube.com/watch?v=9k9KO5WEyog."
142. P.M. Costa, D. Golberg, M. Mitome, Y. Bando, Nitrogen-doped carbon nanotube structure tailoring and time-resolved transport measurements in a transmission electron microscope. Appl. Phys. Lett. **91**, 223108 (2007)
143. L. de Knoop, Investigation of iron filled multiwalled carbon nanotubes, Chalmers University of Technology (Dept. of Applied Physics), 2005
144. M.M. Yazdanpanah, S.A. Harfenist, A. Safir, R.W. Cohn, Selective self-assembly at room temperature of individual freestanding Ag2Ga alloy nanoneedles. J. Appl. Phys. **98** (2005)
145. J. Deneen, W.M. Mook, A. Minor, W.W. Gerberich, C.B. Carter, In situ deformation of silicon nanospheres. J. Mater. Sci. **41**, 4477–4483 (2006)
146. T. Kizuka, R. Kato, K. Miyazawa, Surface breakdown dynamics of carbon nanocapsules. Nanotechnology. **20**, 105205 (2009)
147. R. Zhang, M. Hummelgård, H. Olin, Simple and efficient gold nanoparticles deposition on carbon nanotubes with controllable particle sizes. Mater. Sci. Eng.: B. **158**, 48–52 (2009)
148. R. Zhang, M. Hummelgård, H. Olin, Simple synthesis of clay-gold nanocomposites with tunable color. Langmuir. **26**, 5823–5828 (2010)
149. K.K. Datta, M. Eswaramoorthy, C.N. Rao, Water-solubilized aminoclay-metal nanoparticle composites and their novel properties. J. Mater. Chem. **17**, 613 (2007)

150. O.L. Guise, J.W. Ahner, M. Jung, P.C. Goughnour, J.T. Yates, Reproducible electrochemical etching of tungsten probe tips. Nano Lett. **2**, 191–193 (2002)
151. I. Ekvall, E. Wahlstrom, D. Claesson, H. Olin, E. Olsson, Preparation and characterization of electrochemically etched W tips for STM. Meas. Sci. Technol. **10**, 11–18 (1999)
152. P.M. Costa, X. Fang, S. Wang, Y. He, Y. Bando, M. Mitome, J. Zou, H. Huang, D. Golberg, Two-probe electrical measurements in transmission electron microscopes–behavioral control of tungsten microwires. Microsc. Res. Tech. **72**, 93–100 (2009)
153. J.G. Simmons, Generalized formula for the electric tunnel effect between similar electrodes separated by a thin insulating film. J. Appl. Phys. **34**, 1793 (1963)
154. X.L. Wei, Y. Liu, Q. Chen, L.M. Peng, Controlling electron-beam-induced carbon deposition on carbon nanotubes by Joule heating. Nanotechnology. **19**, 355304 (2008)
155. A.N. Chiaramonti, L.J. Thompson, W.F. Egelhoff, B.C. Kabius, A.K. Petford-Long, In situ TEM studies of local transport and structure in nanoscale multilayer films. Ultramicroscopy. **108**, 1529–1535 (2008)
156. J. Börjesson, *The Role of Interfacial Microstructure of Perovskite Thin Films: A High Resolution and In Situ Study* (Chalmers University of Technology, Sweden, 2009)
157. A. Nafari, P. Enoksson, H. Olin, Si-wedge for easy TEM sample preparation for in situ probing. Eurosensors, Barcelona, 2005
158. D.B. Williams, B.C. Carter, *Transmission Electron Microscopy* (Plenum, New York, 1996)
159. C. Jin, H. Lan, L. Peng, K. Suenaga, S. Iijima, Deriving carbon atomic chains from graphene. Phys. Rev. Lett. **102**, 1–4 (2009)
160. D. Ugarte, Curling and closure of graphitic networks under electron-beam irradiation. Nature **359**, 707–709 (1992)
161. F. Banhart, Irradiation effects in carbon nanostructures. Rep. Prog. Phys. **62**, 1181–1221 (1999)